

Geochemical Controls on Production and Transport of Methylmercury in the St. Louis
River Estuary

A Thesis
SUBMITTED TO THE FACULTY OF THE GRADUATE SCHOOL
OF THE UNIVERSITY OF MINNESOTA
BY

Brian Franklin Beck

IN PARTIAL FULFILLMENT OF THE REQUIREMENTS
FOR THE DEGREE OF
MASTER OF SCIENCE

Nathan W. Johnson

February 2013

© Brian Franklin Beck 2012

Acknowledgements

I would like to thank my advisor, Dr. Nathan Johnson, who provided advice, guidance, and encouragement throughout my graduate career. I would also like to thank my advising committee, Dan Engstrom, Ed Swain, Mike Berndt, and Randall Hicks, who provided intellectual contributions and constructive criticism throughout my project. Finally, I would like to thank my fellow lab-mates Amanda Brennan, Joe Sternberg, Aaron Mika, Nathan Gieske, Mitch Robinson, and Ben Zhu who made long lab hours bearable.

I would like to thank Carl Mitchell's laboratory for conducting total mercury and methylmercury analysis, Ryan Oster for help with SRB qPCR analysis, Steve Kossett for fabricating my voltammetric electrode casings, and the staff of the Civil Engineering Department for help with a myriad of tasks.

This study was funded jointly by the Minnesota Department of Natural Resources' Environmental Cooperative Research Fund, Minnesota's Environment and Natural Resources Trust Fund, and the USGS's Water Resources Research Institute program administered by the Minnesota Water Resources Center.

Dedication

To my family who has provided unending support over the past 27 years and my fiancée, who has stood by my side through thick and thin.

Abstract

The production of methylmercury (MeHg) in freshwater systems is a concern due to its bioaccumulative properties in aquatic food webs and potential neurotoxicity of consumers of fish, including predatory fish, wildlife, and humans. Transformation of inorganic mercury to MeHg is primarily driven by naturally occurring sulfate and iron reducing bacteria (SRB and FeRB) in anoxic sediment and water columns. The first objective of this research was to examine factors known to be important in the production of MeHg (including the quantity and quality of organic carbon, sulfate concentrations, and bioavailability of inorganic mercury to SRB and FeRB) in a historically sulfate-impacted freshwater setting. The second objective was to determine the significance of MeHg flux from sediment to the St. Louis River estuary relative to upstream sources.

A laboratory sulfate addition experiment was performed using 20 cm intact cores obtained from three sites in the St. Louis River estuary. The intact cores from each site were exposed to a high (50 mg/L SO_4^{2-}), control (15 mg/L SO_4^{2-}), and low (5 mg/L SO_4^{2-}) overlying water treatment for an incubation period of six months. Results from this six-month sulfate incubation indicated that when overlying water sulfate concentrations increased to 50 mg/L, MeHg production did not increase in surficial sediment (0 to 4 cm) in any sites. In sediment cores with sulfate concentrations lowered to 5 mg/L in the overlying water, production of sediment methyl mercury did not decrease in surficial sediment (0 to 4 cm); however, the MeHg concentration in sediment from the 4 to 10 cm interval was lower at the end of the six month incubation in sediment from one site. Collectively, results indicate that, in sediment from the St. Louis River estuary, the

quantity and quality of carbon in sediments were more important factors for MeHg production than overlying water sulfate.

In addition to understanding geochemical controls on MeHg production, flux measurements provided a means to compare MeHg loading from sediment relative to MeHg loading from upstream sources. The estimated MeHg loading from habitat zones represented by the three sites included in this study (45% of total estuary area) contributed a small amount MeHg to overlying water relative to upstream sources during low, median, and high flow conditions.

Table of Contents

Contents

Acknowledgements	i
List of Tables	vii
List of Figures	viii
Chapter 1. Introduction and Background	1
<i>Introduction</i>	1
<i>Methyl-Mercury Production and Demethylation</i>	5
<i>Sediment Diagenesis</i>	6
<i>Sulfate Limitation of Mercury Methylation</i>	8
<i>Mercury Porewater Bioavailability</i>	9
<i>Organic Carbon Limitation</i>	10
<i>Sediment Mercury Fluxes</i>	11
Chapter 2 Study Design, Field Methods, and Laboratory Methods	12
<i>Preliminary Site Characterization and Selection</i>	12
<i>Sulfate Amendment Study Site Selection and field methods</i>	14
<i>Preliminary Site Characterization Sediment Sampling and Processing</i>	19
<i>Sulfate Amendment Study Sediment Sampling and Processing</i>	19
<i>Sulfate Amendment Study Porewater Analytical Methods</i>	22
<i>Solid Phase Analysis</i>	25
Chapter 3. Initial Condition Site Characterization	29
Chapter Summary	29
<i>Solid Phase Carbon Concentration and Recalcitrance</i>	29
<i>Initial Porewater Redox Results</i>	32
<i>Solid Phase Acid Volatile Sulfide and Total Sulfur Results</i>	35
<i>Initial MeHg/THg Results</i>	37
<i>Porewater Mercury Partitioning</i>	40
<i>Discussion</i>	44

Chapter 4 Experimental Sulfate Addition Results and Discussion	45
<i>Chapter Summary</i>	<i>45</i>
<i>Experimental Sulfate Loading Results</i>	<i>46</i>
<i>Sulfate Reduction Indicators: SRB Abundance and AVS experimental Results</i>	<i>50</i>
<i>%MeHg Experimental Results</i>	<i>54</i>
<i>Discussion.....</i>	<i>58</i>
Chapter 5 THg and MeHg Transport.....	62
Chapter 6 Conclusions and Implications.....	66
References.....	71
Appendix: Supporting Information	80

List of Tables

Table 1. Primary microbial mediated redox reactions associated with the classical diagenetic model from Fossing (2004).	7
Table 2. Partition Coefficients (K_D) tabulated for THg in the top 10 cm of each habitat zone.	41
Table 3 Partition coefficients (K_D) tabulated for MeHg in the top 10 cm of each habitat zone.	41
Table 4 Porewater MeHg and THg concentrations averaged in each habitat zone (n=3). Overlying water MeHg and THg concentrations from the flux experiments taken at the initial time point (t=0).	64
Table 5 Measured THg and estimated MeHg flux for each habitat zone.	64
Table 6 MeHg and THg loads estimates from each habitat zone. Loads were calculated using areas of fluxes from each habitat zone.	64
Table 7 MeHg and THg concentration measured at the Scanlon Dam in Cloquet taken from Berndt and Bavin (2009). MeHg load calculated from USGS flow data obtained on the same day MeHg water sample was taken.	64
Table S1. AVS, THg, MeHg, %MeHg, Ferrous Iron, dissolved chloride, and dissolved sulfate measured in sacrificial sediment cores used to fill voids created during initial microcosm coring. Each sacrificial microcosm was sub cored to ensure that the geochemical parameters were not markedly different, after which additional sub-cores were used to fill voids created in other microcosms during initial sub-coring.	85
Table S2 Temperature, conductivity, dissolved oxygen (DO), and pH measurements from the overlying water of each sediment core immediately after cores were returned to the lab after field sampling. The LEF and SB habitat zones did not have dissolved oxygen (DO), Conductivity, or temperature recorded during sampling.	86
Table S3. Solid phase and porewater MeHg concentrations from the top 10 cm of each microcosm, which were used to calculate a partition coefficient for each habitat zone.	88
Table S4 Solid phase and porewater THg concentrations from the top 10 cm of each microcosm, which were used to calculate a partition coefficient for each habitat zone.	88

List of Figures

Figure 1. The state of Minnesota with the St. Louis River Watershed boundary highlighted.	2
Figure 2. Vertical structure of microbial reduction and carbon mineralization reactions in the classical diagenetic redox profile found in freshwater systems from Emerson and Hedges 2008.	7
Figure 3. The St. Louis River Estuary with habitat zones delineated by the St. Louis River Alliance. Preliminary site characterization sites (circles) and sulfate amendment study sites (squares), which were sampled in 2010 and 2011, respectively.	13
Figure 4. Sediment core tube attached to sediment corer and drive rod.	15
Figure 5. A schematic of the experimental design with (a) labeled treatment concentrations and (b) a photo of the experimental setup within the temperature control chamber.	18
Figure 6. Initial (0 months) solid phase (a) total carbon (TC) and (b) C/N ratio. Concentrations depicted represent averages (n=3) for each depth section. Horizontal bars represent the standard deviation of the three initial sediment microcosms from each habitat zone. Vertical bars represent the length of section that each data point represents.	30
Figure 7. Initial porewater redox profiles for the LEF ((a)low, (b) control, (c) high), UEF ((d) low, (e)control, and (f)high), and SB ((g)low, (h) control, and (j)high) microcosms. A solid black line (0 cm) denotes the sediment water interface on each sediment profile.	34
Figure 8 . Initial (0 months) (a) solid phase Acid Volatile Sulfides (AVS) and (b) Total Sulfur (TS). Values depicted represent averages (n=3) for each depth section. Horizontal bars represent the standard deviation of the three initial sediment microcosms from each habitat zone. Vertical bars represent the length of section that each data point represents.	36
Figure 9. Initial (0 months) solid phase (a) Total Mercury (THg), (b) Methylmercury (MeHg), and (c) percent methylmercury (%MeHg). Values depicted represent averages (n=3) for each depth section. Horizontal bars represent the standard deviation of the three initial sediment microcosms from each habitat zone. Vertical bars represent the length of section that each data point represents.	38
Figure 10. Relationship between solid phase THg and MeHg for the LEF (diamonds), UEF (triangles), and SB (crosses) habitat zones. R ² value is labeled next to regression line.	39
Figure 11 Average THg partition coefficients and volume weighted average TC and AVS values from the top 10 cm of each sediment microcosm. This figure depicts the influence that AVS and TC have on THg partition coefficients.	43
Figure 12 Sulfate and chloride porewater concentrations for (a and d) SB, (b and e) UEF, and (c and f) LEF habitat zones including overlying water concentrations for high (purple stars), low (pink diamonds), control (brown squares), and initial profiles (blue triangles). A solid black line (0 cm) denotes the sediment water interface on each	

sediment profile. Horizontal bars represent the standard deviation of the three initial sediment microcosms from each habitat zone.	47
Figure 13 Estimated sulfate flux into each sediment microcosm sulfate treatment. Flux values were calculated assuming sediment particle density for LEF, UEF, and SB of 2.5, 2.0, and 1.5 g cm ⁻³ , respectively.....	49
Figure 14. SRB abundance at initial (empty markers; 0 months) and final (black markers; 6 months) laboratory conditions for sediment from (a-high sulfate, d-control sulfate, and g-low sulfate) SB microcosms, (b-high sulfate, e-control sulfate, and h-low sulfate) UEF microcosms, and (c-high sulfate, f-control sulfate, and i-low sulfate) LEF microcosms. Values depicted represent averages (n=3) from triplicate analysis. Horizontal bars represent the standard deviation from triplicate analysis of the DNA extract. Vertical bars represent the composited interval represented by each data point.	51
Figure 15. AVS concentrations at initial (empty markers; 0 months) and final (black markers; 6 months) laboratory conditions for sediment from (a-high sulfate, d-control sulfate, and g-low sulfate) SB microcosms, (b-high sulfate, e-control sulfate, and h-low sulfate) UEF microcosms, and (c-high sulfate, f-control sulfate, and i-low sulfate) LEF microcosms. Horizontal bars represent the standard deviation of the three initial sediment microcosms from each habitat zone. Vertical bars represent the composited interval represented by each data point.	53
Figure 16. Solid phase MeHg, %MeHg, and THg sediment profiles for (a, b, and c) SB, (d, e, and f) UEF, and (g, h, and i) LEF habitat zones at the end of the 6-month experiment. High (purple stars), low (yellow triangles), and control (red squares) overlying water sulfate amendments. Horizontal bars represent the standard deviation of the three initial sediment microcosms from each habitat zone. Points represent samples from 0-4cm, 4-10cm, and 10-20cm intervals.	56
Figure 17 Relationship between % MeHg and TC Abundance for LEF (diamonds), UEF (triangles), and SB (crosses) habitat zones. Data points represent measurements made at the initial and final time points. R ² and p values are labeled next to the regression line they represent.	61
Figure S1 Sediment pH profiles of the initial (empty squares) and final (crosses) conditions for the SB (a), UEF(b), and LEF(c) habitat zones. Final pH measurements were made within a half hour of collection, while initial measurements were made within 3-6 hours of collection.	80
Figure S2. Preliminary data on sediment parameters obtained one year prior to the sulfate addition experiment. Sediment (a) Total organic carbon, (b) total inorganic carbon, (c) porewater sulfate, (d) solid phase AVS, (e) solid phase THg, (f) total sulfur sediment profiles from the Lower Estuary Flats (solid red squares), Clay Influenced Mouth (solid green triangles), and Sheltered Bays (dashed purple crosses).	81
Figure S3 October (+2 months) porewater redox profiles for the LEF ((a)low, (b)control, (c)high), UEF ((d)low, (e)control, and (f)high), and SB ((g)low, (h)control, and (j)high) microcosms. A solid black line (0 cm) denotes the sediment water interface on each sediment profile.....	82

Figure S4 January (+4 months) porewater redox profiles for the LEF ((a)low, (b)control, (c)high), UEF ((d)low, (e)control, and (f)high), and SB ((g)low, (h)control, and (j)high) microcosms. A solid black line (0 cm) denotes the sediment water interface on each sediment profile..... 83

Figure S5 February (+6 months) porewater redox profiles for the LEF ((a)low, (b)control, (c)high), UEF ((d)low, (e)control, and (f)high), and SB ((g)low, (h)control, and (j)high) microcosms. A solid black line (0 cm) denotes the sediment water interface on each sediment profile. 84

Figure S6 Overlying water in each microcosm was monitored for sulfate and chloride on a bi-weekly basis and is depicted in this figure..... 87

Chapter 1. Introduction and Background

Introduction

The St. Louis River watershed is located in northeastern Minnesota and drains into Lake Superior near Duluth, Minnesota (Figure 1). The total drainage area of the St. Louis River is 9,283 km², with a total length of 313 km from its source (Lindgren et al. 2006). The main stem of the St. Louis River follows a C-shaped pattern, beginning in the northeast region of the watershed and drains into Lake Superior at the southeast region of the watershed (Figure 1). The St. Louis River basin contains large areas of wetland (16% of the total watershed area) resulting in relatively high concentrations of dissolved organic carbon (DOC) (10-40 mg/L) (Berndt and Bavin 2012).

Historically, the St. Louis River has been impacted by iron mining activities (beginning in the late 19th century) in the upper reaches of the watershed, which has led to elevated surface water sulfate concentrations (Lindgren et al. 2006). Historic and ongoing mining activities have not resulted in low pH and elevated dissolved metals due to the relatively low sulfur content in ores compared to acid-neutralizing carbonate and silicate minerals in the Mesabi Iron formation. Due to sulfide mineral oxidation in mine waste rock and subsequent runoff into tributaries, sulfate loading from mining impacted watersheds is high relative to unimpacted tributaries (Berndt and Bavin 2009). Sulfate concentrations in the main stem of the St. Louis River are dependent on two factors:

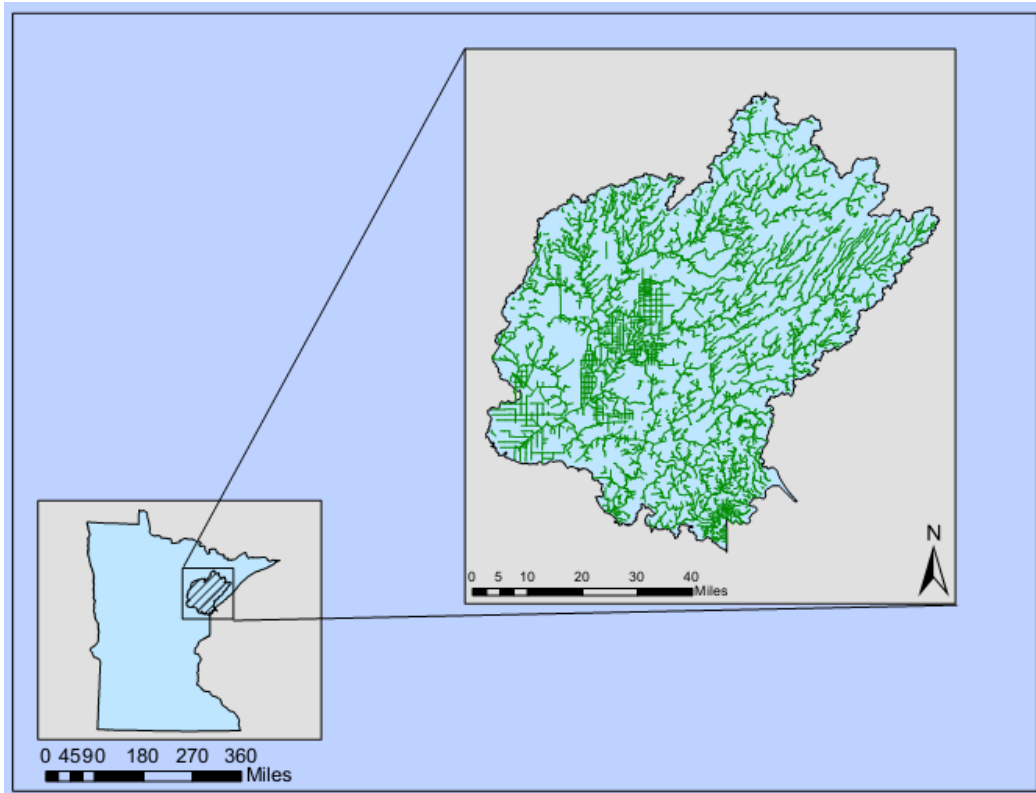


Figure 1. The state of Minnesota with the St. Louis River Watershed boundary highlighted.

(a) proximity to mining impacted tributaries and (b) river discharge (Berndt and Bavin 2009). Main stem sulfate concentrations increase below the confluence of impacted tributaries and are diluted downstream by unimpacted tributaries (Berndt and Bavin 2009^{a,b}). Temporally, sulfate concentrations are higher during low flow conditions and lower during high flow conditions but continuously remain above background levels in local streams draining unimpacted watersheds (2-7mg/L).

Sulfate is a concern in the St. Louis River watershed, not because of its direct toxicological effects, but due to its role in transforming inorganic mercury to methylmercury (MeHg). Currently, there is a fish consumption advisory in the St. Louis River estuary due to elevated mercury concentrations in fish tissue (WI DNR 2011). It has been shown that mercury methylation is biologically mediated by sulfate reducing bacteria (Compaeu and Bartha 1985), which require inorganic mercury, organic matter, sulfate, and anoxic conditions in order to produce MeHg. In low-sulfate freshwater aquatic systems, it has been demonstrated that varying sulfate concentrations influences the production of MeHg (Gilmour et al. 1992; Jeremiason et al. 2006), however, the biogeochemical processes controlling MeHg production by SRB are complex and a direct relationship between sulfate and MeHg production does not always exist (Benoit et al. 2003). Since sulfate in the overlying water (Berndt and Bavin 2009) and MeHg in fish tissue (WI DNR 2011) are elevated in the St. Louis River estuary, understanding whether sulfate concentrations in the overlying water are important in driving mercury methylation in sediments is a necessary step for defining management solutions aimed at reducing methylmercury in fish tissue.

In addition to production, the transport of MeHg out of sediment is an important factor that may influence the quantity of MeHg delivered to the overlying water, where it can bioaccumulate in biota (Hammerschmidt et al. 2004^b; Benoit et al. 2009). Although sediment is a potential source of MeHg throughout the St. Louis River, it is of particular concern in the estuary due to longer residence times. The widening of the river in the estuary slows the flow of water and allows for a longer duration of sediment–water interaction, which may allow greater accumulation of MeHg in the overlying water. Currently, there have been no attempts to measure MeHg flux out of the sediment in the St. Louis River estuary to determine if sediment is an important contributor of MeHg to the overlying water. Without knowledge of MeHg loading to the overlying water from sediment, it is difficult to establish the relative importance of different sources of MeHg to the St. Louis River estuary.

This study sought to understand whether the production of methylmercury in sediment was influenced by overlying water sulfate in a freshwater estuary system historically impacted by sulfate. To determine whether mercury methylation in sediment from various habitats of the St. Louis River estuary was influenced by sulfate, a laboratory sulfate addition experiment was conducted. Unlike other sulfate addition experiments that have used sediment slurries (Harmon et al. 2007; Gilmour et al. 1992), this study utilized intact sediment cores to understand how overlying water sulfate concentrations influence MeHg production. Studying intact sediment cores maintained realistic redox porewater conditions that were more representative of field conditions relative to sediment slurries. In addition to studying MeHg production, MeHg fluxes

were estimated to determine if sediment could contribute a significant amount of MeHg to overlying water in the estuary.

Methyl-Mercury Production and Demethylation

The transformation of inorganic mercury to methylmercury has been shown to be primarily microbially mediated (Compau and Bartha 1985; Gilmour et al. 1992; Kerin et al. 2006; Fleming et al. 2006). Sulfate reducing bacteria (SRB) are widely considered the primary methylators of mercury in aquatic sediments (Gilmour et al. 1992; Jeremiason et al. 2006), although iron-reducing bacteria (FeRB) have demonstrated the ability to methylate mercury in pure cultures (Fleming et al. 2006; Kerin et al. 2006). Recently, it was demonstrated that SRB and FeRB collectively methylate mercury in some sediments, which has expanded the classic, SRB-exclusive, methylation model (Yu et al. 2012).

In environmental systems, MeHg is also demethylated through biotic and abiotic reactions, and the balance between methylation and demethylation processes results in steady-state MeHg concentrations in sediment. Microbial MeHg degradation is the dominant demethylation pathway in sediment systems (Benoit et al. 2003), while abiotic photodegradation and oxidative demethylation play a less influential role in the degradation of MeHg in anoxic sediment (Sellers et al. 1996; DiPasquale et al. 2000).

In anoxic sediments, mercury methylation and demethylation are concurrent processes that are often assumed to be in steady-state under field conditions. Since solid phase MeHg and THg concentrations are thought to be the result of a balance between methylation and demethylation rates, the fraction of total mercury present as MeHg (%MeHg) in the solid phase can be considered a good measure of net MeHg production

in sediment systems (Drott et al. 2008).

Sediment Diagenesis

In aquatic sediments, the consumption of oxidized compounds acting as terminal electron acceptors in microbially mediated reactions occurs in a sequential pattern with depth (Froelich et al. 1979) (Figure 2). Due to the Gibbs free energy associated with each reaction (Stumm and Morgan 1996) (Table 1) the characteristic order of electron acceptor consumption in sediments is oxygen (O_2) first, followed by nitrate (NO_3^-), manganese (Mn^{4+}), ferric iron (Fe^{3+}), sulfate (SO_4^{2-}), and then organic matter (Table 1). These electron acceptors are continuously transported from the overlying water to the sediment by diffusion or depositional processes and consumed at depth by specific microbial populations. The depth at which an oxidized electron acceptor penetrates into the sediment depends on the favorability of the redox reaction. This sequence of microbial reactions, termed diagenesis, is responsible for reducing the aforementioned electron acceptors and oxidizing organic matter (Jorgensen 1982).

The primary driver of sediment diagenesis in aquatic systems is organic carbon delivered to the sediment surface (Meyers and Ishiwatari 1993). In organic rich sediment, there tends to be a compression of the diagenetic microbial communities upwards, towards the sediment-water-interface (SWI) due to rapid rates of microbial activity. Conversely, in organic-poor aquatic systems, redox zones are stretched out, allowing deeper penetration of oxidized electron acceptors into the sediment (Katsev et al. 2006). In addition to the concentration of organic carbon, the quality of organic

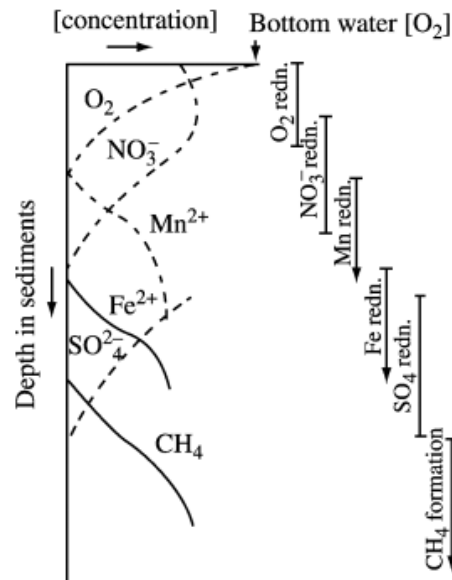


Figure 2. Vertical structure of microbial reduction and carbon mineralization reactions in the classical diagenetic redox profile found in freshwater systems from Emerson and Hedges 2008.

Table 1. Primary microbial mediated redox reactions associated with the classical diagenetic model from Fossing (2004).	
Aerobic Respiration:	$\text{CH}_2\text{O} + \text{O}_2 \rightarrow \text{CO}_2 + \text{H}_2\text{O}$
Nitrate Respiration:	$4\text{NO}_3^- + 5\text{CH}_2\text{O} + 4\text{H}^+ \rightarrow 2\text{N}_2 + 5\text{CO}_2 + 7\text{H}_2\text{O}$
Manganese Reduction:	$2\text{MnO}_2 + \text{CH}_2\text{O} + 4\text{H}^+ \rightarrow 2\text{Mn}^{2+} + 3\text{H}_2\text{O} + \text{CO}_2$
Iron Reduction:	$4\text{FeOOH} + \text{CH}_2\text{O} + 8\text{H}^+ \rightarrow 4\text{Fe}^{2+} + \text{CO}_2 + 7\text{H}_2\text{O}$
Sulfate Reduction:	$\text{SO}_4^{2-} + 2\text{CH}_2\text{O} + 2\text{H}^+ \rightarrow \text{H}_2\text{S} + 2\text{CO}_2 + 2\text{H}_2\text{O}$
Methanogenesis:	$2\text{CH}_2\text{O} \rightarrow \text{CH}_4 + \text{CO}_2$

carbon can limit or enhance the microbial rates of diagenesis (Meyers and Ishiwatari, 1993). The type of organic carbon transported to sediment can be placed into two general categories, autochthonous and allochthonous carbon. The difference between the two types of organic carbon is that autochthonous carbon is produced at the site in which it is deposited while allochthonous carbon is transported to the site of deposition (Wetzel 2002). Because allochthonous organic carbon in fluvial systems is degraded by microbial and macrobiotic processes during transport, this type of organic carbon tends to be more refractory (Vannote et al. 1980). Both the quantity and quality of organic carbon in sediments influence overall microbial activity including sulfate reduction.

Sulfate Limitation of Mercury Methylation

A number of studies have shown that the addition of sulfate to a low sulfate system can enhance methylmercury production by stimulating SRB (Branfireun et al. 1999; Gilmour et al. 1992; Jeremiason et al. 2006; Harmon et al. 2004). Proxies that have been used to measure the response of SRB to sulfate addition include sulfate reduction rate (SRR), microbial community characterization, sulfide concentration change, CO₂/CH₄ production, and acid volatile sulfide concentration change (King et al. 1999; King et al. 2000; Benoit et al. 2003).

Some sulfate addition experiments have been conducted in homogenized sediment amended with sulfate (sediment slurries) or in pure cultures of specific SRB (Harmon et al. 2007; Gilmour et al. 1992; King et al. 2000). These studies were useful for determining the mediator of MeHg production in sediment but did not replicate intact diagenetic redox zones in which they were collected. Other studies have examined field-

scale sulfate additions to low-sulfate, freshwater wetland ecosystems, which resulted in significant MeHg production after sulfate additions (Jeremiason et al. 2006; Coleman-Wasik et al. 2012). While performed in field conditions, the sulfate addition in these studies represented changes in periodic atmospheric sulfate loads from precipitation, not a continuous change to overlying water column concentrations.

Although MeHg production can be limited by sulfate, other geochemical factors such as availability of labile organic carbon, porewater inorganic mercury concentration and bioavailability, and competition among microbial communities can influence methylation (Hammershmidt et al. 2004^a; Drott et al. 2007; Todorova et al. 2009). A conceptual model more complex than simple sulfate-driven MeHg production is required to adequately explain mercury dynamics in the context of an intact sediment column.

Mercury Porewater Bioavailability

The quantity and speciation of mercury in sediment porewater has a large influence on the ability of a system to produce MeHg efficiently (Benoit et al. 2003). Observations of systems with elevated sulfide concentrations and muted MeHg production provided early evidence of sulfide's influence on MeHg production (Gilmour et al. 1998; Benoit et al. 1999^a). Geochemical equilibrium modeling suggests that increasing sulfide concentration decreases the concentration of uncharged mercury-sulfide complexes (HgS^0 and HgSHOH^0) that may diffuse passively across cell membranes of SRB to be methylated (Benoit et al. 1999^a). Dissolved organic matter (DOM) with thiol groups have also been proposed as strong ligands for complexing inorganic mercury (Skylberg 2008). In addition to uncharged mercury-sulfide compounds, low molecular weight

organic compounds are capable of complexing mercury and may be transported into the methylating bacteria via active transport (Golding et al. 2002) and colloidal sulfide nanoparticles could also be important in dissolved mercury speciation (Deonarine and Hsu-Kim 2009).

Iron sulfide complexes may also have a role in reducing the concentration of porewater inorganic mercury (Skylberg 2008; Skylberg and Drott 2010). Iron sulfide solids have the ability to remove inorganic mercury from the dissolved phase, which has been demonstrated experimentally with pyrite (FeS_2) (Bower et al. 2008; Liu et al. 2008). Iron sulfide dynamics with mercury are not well understood and more investigation is needed to accurately model FeS limitation of porewater inorganic mercury availability to SRB.

Organic Carbon Limitation

Organic carbon is used as an electron donor for chemoheterotrophic bacteria (Froelich et al. 1979). The addition of labile organic carbon can yield high mercury methylation rates, if sulfate is not limiting SRB metabolism (Mitchell et al. 2008^a). Carbon to nitrogen ratios (C/N ratio) have been employed to quantify the quality of organic carbon in salt water systems (Kim et al. 2011) in the context of mercury methylation.

Solid-phase organic carbon can also have a negative effect on the production of MeHg by lowering porewater concentrations of inorganic mercury (Hammersmidt et al. 2004^a). Organic carbon in sediment is highly correlated with mercury partitioning coefficients (K_D – the ratio of adsorbed to dissolved mercury), such that high solid-phase

carbon typically reduces the porewater mercury available to microbial populations (Hammerschmidt et al. 2004^a). However, if the organic carbon is labile, a larger abundance of organic carbon can increase MeHg production (Lambertsson and Nilsson 2006). Understanding the quality of the total carbon pool can assist interpretations between carbon's effect on stimulating microbial populations and carbon's effect on mercury partitioning.

Sediment Mercury Fluxes

Anoxic sediment has proven to be an important location of MeHg production in freshwater and marine systems (Hammerschmidt et al. 2004^a; Yu et al 2012; Gilmour et al. 1992). However, biota are only exposed to MeHg in surficial sediment or if it is transported to the overlying water column. Multiple methods have been used to estimate and measure MeHg flux across the sediment-water interface, including in-situ benthic flux chambers (Gill et al. 1999; Choe et al. 2004), sediment core incubations (Hammerschmidt et al. 2008; Mason et al. 2006), and diffusive transport estimates from porewater mercury profiles (Hammerschmidt et al. 2004^b; Choe et al. 2004). It has been observed that diffusive transport models commonly underestimate MeHg flux relative to measured fluxes (Choe et al. 2004; Covelli et al. 1999). The disparity between flux measurements and diffusion calculations has been attributed to systems in which bioturbation by benthic fauna plays an important role in MeHg transport (Hammerschmidt et al. 2008; Benoit et al. 2009). In addition to the effect of biotically-enhanced MeHg transport, thermodynamic modeling suggests that under certain

geochemical conditions uncharged MeHg sulfur complexes may enhance the transport of MeHg into the water column (Jonsson et al. 2010).

Chapter 2 Study Design, Field Methods, and Laboratory Methods

Preliminary Site Characterization and Selection

The objective of the preliminary site characterization study was to measure sediment geochemical parameters in the St. Louis River estuary to help inform site selection for the sulfate amendment laboratory study. Results from this study were not included in the text of this document, but are depicted in Figure S2. In an attempt to choose a limited number of sites that could represent a large portion of the estuary, habitat zones delineated by the St. Louis River Alliance (SLRA 2002) were employed (Figure 3). Three sites were selected from habitat zones that collectively covered 38% of the estuary and were expected to exhibit a range of carbon quantity and quality (Crane 2006). The habitat zones selected for the preliminary characterization were the lower estuary flat (LEF), clay influenced mouth (CIM), and shelter bay (SB) (Figure 3). Five cores with intact sediment water interfaces were obtained in October 2010 from each field site using a piston corer equipped with 6.35 cm diameter polycarbonate core tube. Cores were stored vertically at 4° C for 1 to 7 days until sectioning. Results from the preliminary site characterization study demonstrated that there were differences among sites with regard to solid phase total mercury and organic carbon (Figure S2). In

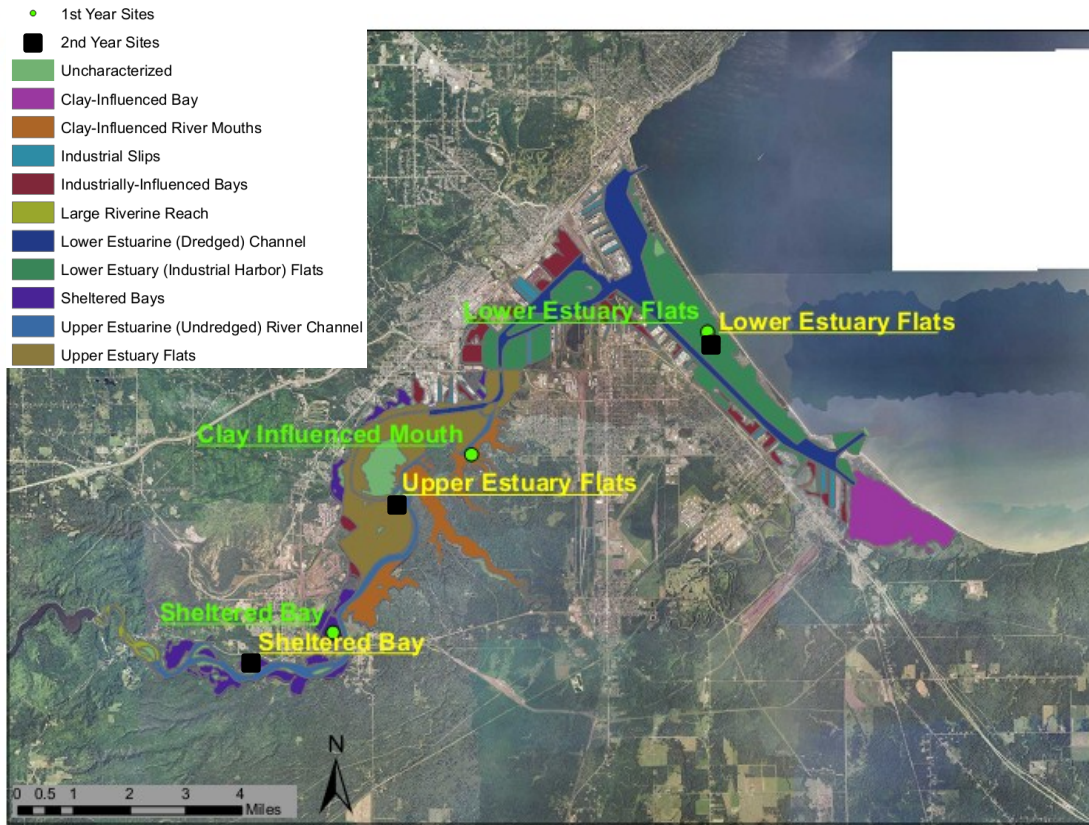


Figure 3. The St. Louis River Estuary with habitat zones delineated by the St. Louis River Alliance. Preliminary site characterization sites (circles) and sulfate amendment study sites (squares), which were sampled in 2010 and 2011, respectively.

addition, sulfate was consumed within the top 5 to 10 cm in all sites suggesting that biological sulfate reduction was occurring in that interval of the sediment column. MeHg for the preliminary site characterization was measured but not reported due to low analytical laboratory spikes and problems during storage.

Sulfate Amendment Study Site Selection and field methods

Habitat zones were selected for the sulfate-addition study in light of information gathered during the preliminary site characterization and included the Lower Estuary Flat (LEF), Upper Estuary Flat (UEF), and Sheltered Bay (SB) habitat zones. These sites (a) cover 21%, 17%, and 7% of the St. Louis River estuary, respectively (SLRA 2002), (b) contain a range of organic carbon solid phase concentrations (Figure S2), and (c) were not influenced by regular dredging operations. Although other habitat zones covered larger areas of the estuary than those selected, they were highly influenced by industry or dredging activity making representative site selection difficult. In addition, the two sites selected for study (Lower Estuary Flat and Sheltered Bay) were known to contain a range of solid phase organic carbon (<1% to ~5% TOC, respectively; Figure S2).

Four sediment cores were collected from each of the three field sites in August 2011 using a clean 20 cm inner diameter polycarbonate tube. The sediment corer (Figure 4) was driven into the sediment using a drive rod operated from the sampling boat. Once the core tube penetrated 20 to 30 cm into the sediment, two ball valves, which were open



Figure 4. Sediment core tube attached to sediment corer and drive rod.

during penetration, were shut to create a seal that would preserve the sediment-water interface as the core was removed from the sediment. Meanwhile, the bottom of the core was capped after extraction with an o-ring-fitted polyethylene disk. Twelve sediment cores were transported to the laboratory where dissolved oxygen and pH (Table S 2) were measured in the overlying water. Afterwards, two holes were drilled into the polycarbonate tubing 10 cm above the sediment-water interface, directly across from one another. Each hole in the polycarbonate tubing was fitted with 6.35 mm polyethylene hose barbs. Within 4 hours of collecting the sediment cores, oxygenated water from each sample site was pumped through the barbed fittings over the cores at 100 mL min^{-1} to ensure that water near the sediment-water interface did not become anoxic. The cores were stored at 20°C for one week in a climate control chamber with recirculating overlying site water before initial characterization was performed.

Initial characterization included scanning each microcosm with voltammetric electrodes to measure porewater redox conditions (Mn^{2+} , Fe^{2+} , S^{2-} , and O_2) (Brendel et al. 1995). Triplicate sub-cores were extracted to obtain vertical profiles of solid phase and other porewater concentrations. These methods were also used to analyze the final conditions in the sediment microcosms at the end of the six-month study. A detailed description of lab methods is included in the following sections.

Once initial conditions for each microcosm were measured, water from the initial interface was replaced by experimental sulfate treatments. All overlying water sulfate treatments were made from Cloquet River water since it contained dissolved organic carbon (DOC) concentrations similar to the main stem of the St. Louis River (18-40 mg

L⁻¹ DOC) and low sulfate concentrations (2.5-5 mg L⁻¹) (Berndt and Bavin 2009). Cores from each habitat zone had overlying water containing three different sulfate concentrations (Sodium Sulfate added to Cloquet River water) recirculated for a period of six months. Fresh Cloquet water was obtained and amended every two months during the laboratory study. The six-month incubation period was selected considering diffusion calculations made prior to field sampling, which estimated that six months was a sufficient amount of time for sulfate in the overlying water to diffuse approximately 10 cm into the sediment.

Sulfate concentrations in the overlying waters were adjusted to 50 mg L⁻¹ (high treatment), 15 mg L⁻¹ (control treatment), and 5 mg L⁻¹ (low treatment), respectively, which were thought to simulate environmentally relevant concentrations in the St. Louis River estuary (Figure 5). The high sulfate treatment was meant to simulate a situation where sulfate loading to the estuary increased. The control sulfate treatment was determined by estimating the sulfate concentration during median discharges at the upper end of the St. Louis River estuary (USGS station 04024000). The median discharge at the gauging station for August (1,290 ft³ s⁻¹) was then compared to discharges and sulfate concentrations measured by Berndt and Bavin (2009) to determine an average sulfate concentration that would be used for the control treatment (15 mg L⁻¹). Little spatial variation in sulfate concentration within the estuary was reported in the summer of 2010 (Axler and Hobbs, unpublished data). The low treatment (5 mg L⁻¹ sulfate) was chosen based on sulfate measurements reported for local, unimpacted subwatersheds, such as the Cloquet River (Berndt and Bavin, 2009), which could occur if sulfate loading decreased.

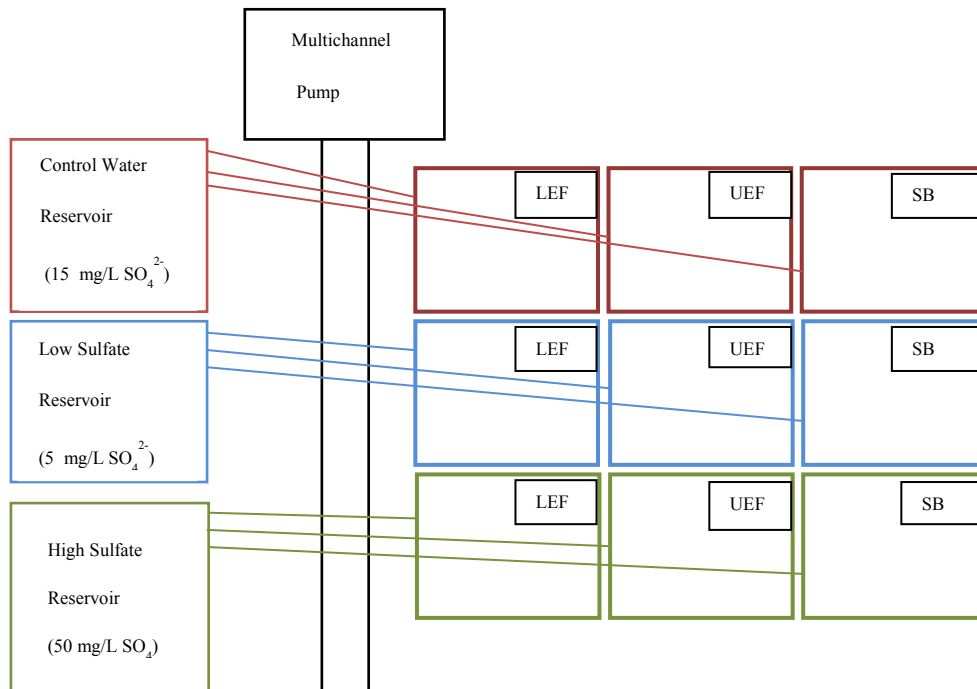


Figure 5. A schematic of the experimental design with (a) labeled treatment concentrations and (b) a photo of the experimental setup within the temperature control chamber.

Preliminary Site Characterization Sediment Sampling and Processing

Cores collected during the preliminary site characterization were extruded and sectioned into 1.5 cm intervals from 0 to 6 cm, 2 cm intervals from 6 to 14 cm, 5 cm intervals from 14 to 29 cm, and 10 cm intervals from 29 to 49 cm. Sediment sections were transferred into acid-cleaned glass jars, which were subsequently transferred to a nitrogen atmosphere for homogenization and sub-sampling. Solid phase acid volatile sulfides were analyzed using a method outlined in Brouwer et al. (1994). Porewater was extracted by centrifuging sediment in 50 mL polypropylene centrifuge tubes for 30 minutes at 10,000 rpm. Porewater for sulfate determination was then subsampled and filtered in a nitrogen atmosphere. Sediment was also subsampled with a Parafilm-covered stainless steel spatula for total Hg (THg) measurements and placed into 20 mL scintillation vials that had been cleaned in 10% HNO₃. THg samples were stored at -20°C until they were sent to an analytical laboratory (Steve Balogh, Met Council, St. Paul, MN) for measurement. A small aliquot of sediment (10 g) was placed in a 20 mL scintillation vial and freeze-dried for solid phase total organic carbon (TOC) and total sulfur (TS) determination.

Sulfate Amendment Study Sediment Sampling and Processing

For the sulfate amendment study, each 20 cm diameter sediment microcosm was sub-cored in triplicate using 2.54 cm diameter polycarbonate tubing following the one-week laboratory storage period. Sub-cores were extruded using a 2.23 cm diameter polyethylene rod wrapped with electrical tape to ensure a secure fit inside the sub-coring

tube. A 3.02 cm butyl tube was inserted into the sediment prior to sub-coring to prevent the sediment from falling into the void created by the sub-core. Sediment was sectioned into 0 to 4 cm, 4 to 10 cm, and 10 to 20 cm intervals and placed directly into trace-metal clean glass jars. Each sediment sample jar was immediately filled with nitrogen gas to minimize the alteration of redox conditions. Within 15 minutes of microcosm sub-coring, sample jars were placed in a Coy anaerobic chamber with an oxygen-free atmosphere (97.5% nitrogen and 2.5 % hydrogen) where samples were homogenized and sub-sampled for solid-phase and porewater analysis. Any solid-phase sub-samples that were not analyzed within 12 h of sub-coring were stored at -20°C.

To preserve the vertical structure of the microcosm sediment during initial characterization, sub-cores (2.54 cm diameter) from a sacrificial microcosm (20 cm diameter) were used to fill each hole from which an analytical sub-core was removed. To ensure that sediment being added to the microcosms from the sacrificial cores was not substantially different; the sacrificial core was also sub-cored and analyzed to determine its solid phase and porewater profile concentrations (**Error! Not a valid bookmark self-reference.**). To determine the within-microcosm variability, triplicate sub-cores in one microcosm for each habitat zone were analyzed separately during initial characterization. Horizontal error bars on each figure displaying analytical results from the sulfate amendment study represent one standard deviation of the triplicate measurements made (at each respective depth) during initial characterization. In microcosms that did not have individual triplicate sub-cores analyzed, sub-cores were composited at each respective depth (0 to 4, 4 to 10, and 10 to 20 cm).

Partition coefficients for total mercury (THg) and methylmercury (MeHg) were determined by measuring solid phase and dissolved (sample passing 0.45 μm polyethersulfone filter) mercury at the close of the experiments. A polycarbonate sub-core (6.35 cm) was removed from each microcosm after which the top 10 cm was extruded into a 3.8 L Ziploc sample bag and transferred into an oxygen free atmosphere. Each sediment sample was homogenized thoroughly and transferred into 50 mL polypropylene centrifuge tubes (multiple tubes were required per microcosm). The sediment was centrifuged (10,000 rpm for 30 min) after which it was immediately filtered through a polyethersulfone filter (0.45 μm -pore size) into clean PETG bottles and acidified using ACS trace-metal grade hydrochloric acid (0.5%). A small subsample of homogenized sediment was removed before centrifuging and placed in a trace-metal clean scintillation vial for solid phase THg and MeHg analysis.

At the conclusion of the experiments, THg flux was measured in each microcosm. For these measurements, fresh Cloquet River water was obtained in 50 L acid-cleaned carboys. Five volumes of water (3.14 L = one volume) were allowed to flow over each microcosm at a predefined rate to ensure fresh Cloquet River water was sitting on top of each microcosm. Then, flow ceased and the water sat on top of the sediment for 36 to 48 h with a small stream of air bubbling through PTFE tubing to mix overlying water and maintain oxic conditions. After 36 to 48 hours, the overlying water was sampled with trace-metal, nitric-acid cleaned polypropylene syringes, and filtered through disposable 0.45 μm -pore polyethersulfone filters directly into PETG trace-metal-clean bottles. All samples were acidified with 0.5% ACS trace-metal hydrochloric acid. Both solid phase

and liquid phase total- and methyl- mercury samples for the sulfate addition study were analyzed in the lab of Carl Mitchell at the University of Toronto Scarborough.

Sulfate Amendment Study Porewater Analytical Methods

Dissolved sulfide ($\Sigma S^{2-} = H_2S + HS^- + S^{2-}$), ferrous iron (Fe^{2+}), oxygen (O_2), and manganese (Mn^{2+}) were measured using mercury gold amalgam voltammetric electrodes following methods similar to Brendel et al. (1995). Electrodes were constructed with epoxy casings produced using stereolithography rapid prototyping (UMD-NRRI Northern Lights Technology Center). The inner copper wire of a coaxial cable was soldered to a 100 μm diameter gold wire and inserted into the epoxy casing. Subsequently, the casing was filled with non-conductive epoxy resin. The epoxy resin was allowed to harden for 24 h after which a BNC connector was attached to coaxial cable to enable connectivity to the potentiostat (Analytical Instrument Services Inc., Flemington, NJ).

The end of each electrode was polished using a 600 grit abrasive sheet followed by 800 grit abrasive sheet to provide a flat surface for ultra-fine polishing. Following the abrasive surface polishing, 15 μm , 6 μm , 1 μm , and 0.25 μm diamond polishes (Buehler Company) were used in sequence on nylon and micro-cloth pads to provide a smooth gold surface for Hg(0) plating. Once polishing was complete, electrodes were cleaned with acetone and distilled water to ensure a clean surface for optimal plating. Polished electrodes were visually inspected using a microscope (100x magnification) to confirm the quality and cleanliness of the electrode surface. Then, the electrode tip was submerged in liquid Hg(0) for 12 h to obtain a thorough plating on the gold wire surface. Nitric acid

(10% HNO₃) was used to clean off recently plated electrodes to remove any excess Hg(0) remaining on the end of the electrode surface that was not directly plated on the polished gold wire. Each electrode was then inspected using a microscope to ensure a mercury hemisphere with few imperfections had amalgamated to the gold wire. The plated electrode surface was stored in DI water until analysis to ensure the mercury surface did not dry.

Manganese (MnCl₂·4H₂O) and iron (FeCl₂·4H₂O) stock solutions were prepared weekly in Millipore (18.2 MΩ/cm) water with the pH adjusted to 4.0 using nitric acid, while sulfide (Na₂S·9H₂O) stock solutions were adjusted to pH 10 using sodium hydroxide (NaOH). When calibrating electrodes for Mn²⁺ and Fe²⁺, a filtered Cloquet River water matrix was used with 0.6 mM and 1.2 mM acetic acid buffer (pH 4.48), respectively. Sulfide calibrations were also conducted in a Cloquet River water matrix using 1.2 mM HEPES buffer (pH 8.6). A two-point oxygen calibration was performed in unamended Cloquet River water, assuming saturated oxygen concentrations initially and zero oxygen after N₂ bubbling for 15 to 20 minutes. All anoxic calibration (Mn²⁺, O₂, Fe²⁺, and ΣS²⁻) solutions were degassed by purging the solution with nitrogen gas at 80 mL min⁻¹ for 15 to 20 min and maintaining N₂ in headspace during analysis.

Square wave voltammetric scans used for ΣS²⁻, Mn²⁺, and Fe²⁺ that consisted of a potential range of -0.1 to -2.1 volts (V) vs a silver/silver chloride (Ag/AgCl) reference electrode, 15 mV step height, and 200 mV s⁻¹ scan rate. In the presence of sulfide, a -0.8 V conditioning step was applied for 10 to 30 sec before the acquisition scan, while in the presence of Mn²⁺ and Fe²⁺ a -0.2 V conditioning step was applied for 10 to 30 sec to

remove any iron, manganese, or sulfur deposited during scans. Oxygen was determined with linear sweep voltammetric scans across a range of -0.1 to -1.8 mV using a 200 mV s⁻¹ scan rate.

All porewater samples other than those measured using voltammetric electrodes were obtained by removing a sub-sample from a homogenized sediment section under a N₂ atmosphere. These subsamples were centrifuged at 10,000 rpm for 30 min in 50 mL polypropylene centrifuge tubes. Supernatant was then poured into 15 mL polypropylene syringes and filtered through 0.45 µm polyethersulfone filters directly into acid cleaned 15 mL polypropylene centrifuge tubes for short-term storage in an N₂ atmosphere in order to decrease the potential of changes in redox conditions.

A 10 mL aliquot from the centrifuge-extracted porewater was removed and acidified to pH 4.5 to convert all dissolved sulfide species (H₂S, HS⁻, and S²⁻) to H₂S, which reduces the amount of sulfide available to oxidize to sulfate prior to analysis by Ion Chromatography. After acidification, samples were placed in 5 mL Dionex polyvials with 20 µm-pore filter caps and loaded into a Dionex ICS-1100 Integrated IC system (AS-DV Autosampler). Each sample was injected into the 25 µL sample loop, which was separated using a Thermo Scientific AS22 IonPac 4x250 mm anion exchange column, after which each anion passed through the conductivity cell for detection. The eluent was 4.5 mM sodium carbonate and 1.4 mM sodium bicarbonate pumped at a rate of 1.2 mL min⁻¹. The suppressor current was set at 31 nA and the column was continuously heated at 30° C. Sulfate and chloride standards were made using sodium sulfate (Na₂SO₄) and sodium chloride (NaCl) in Millipore water, and were checked

against a Thermo Scientific anion standard. Porewater pH was measured in filtered samples before any acidification with a VWR Symphony pH electrode following a 3-point calibration (pH 4, 7, and 10).

Solid Phase Analysis

Acid volatile sulfide (AVS) was measured in the sediment solid phase using the Brouwer Diffusion Method (Brouwer and Murphy 1994). A quantitative amount of sediment (~0.5 g) was placed in the bottom of a 20 mL scintillation vial in an oxygen-free atmosphere. A 2 mL microcentrifuge tube containing 1.0 mL of sulfide antioxidant buffer (SAOB) was placed inside the 20 mL scintillation vial containing the sediment sample. The SAOB contained Ethylenediaminetetraacetic acid (EDTA), ascorbic acid, and sodium hydroxide (NaOH) (Eaton et. al. 2005). After placing both sediment and the 1.0 mL microcentrifuge tube of SAOB in the scintillation vial, a gas tight Supelco Mininert septa cap with valve was used to seal the vial. Once the scintillation vial was sealed, 5 mL of 50 mM oxalic acid in a 2 N HCl solution was injected through the gas tight septa into the scintillation vial using a stainless steel 20 gauge hypodermic needle. The samples were placed on an orbital shaker (intermediate speed setting) for 4 h in a dark environment. After 4 h, the inner SAOB centrifuge tube was removed and diluted to 3 mL with SAOB.

A sulfide ion-specific electrode (ISE) was used to measure the sulfide concentrations of the solid phase extract in each SAOB tube. The sulfide ISE was calibrated using a sulfide stock solution made with sodium sulfide ($\text{Na}_2\text{S}\cdot 9\text{H}_2\text{O}$) and

Millipore water (pH 10), which was then diluted in a SAOB matrix to create calibration standards. Sulfide stock solution was stored in an oxygen-free atmosphere and checked using an iodometric titration if stock had been prepared more than a month prior to analysis (Eaton et. al. 2005). AVS extract concentrations quantified by ISE were converted to solid phase dry mass concentrations using water content. Dry mass and water content were determined for each homogenized sediment section by placing ~1 g of sediment on a pre-weighed aluminum dish. Samples were immediately weighed and placed in a 105° C oven for 24 h. Sediment samples were then reweighed to determine dry mass. All solid phase results were normalized to dry weight.

Preliminary site characterization sediment samples were freeze dried prior to elemental analysis and kept in a desiccator to remove any moisture before analysis. Solid phase total organic carbon (TOC) and total sulfur (TS) were analyzed using a UIC Corporation CO₂ and SO₂ coulometer. First, total inorganic carbon (TIC) was measured by acidifying sediment samples using dilute HCl, driving off carbonates as CO₂ that were measured by a electrochemical coulometric cell. Total carbon (TC) was then measured by placing a known mass of sediment into a ceramic boat (without HCl addition), which was inserted into a 950° C combustion furnace that converts all carbon (inorganic and organic) to CO₂. The CO₂ was measured by the same electrochemical coulometric cell. Total Inorganic Carbon (TIC) was subtracted from TC to determine TOC concentrations. For TS analysis, a known amount of sediment was placed in a ceramic boat and covered with vanadium pentoxide in stoichiometric excess to drive sulfur combustion to completion in the combustion chamber (1050° C).

Sediment samples analyzed for total sulfur (TS), total nitrogen (TN) total carbon (TC) for the sulfate amendment study were dried for 48 h in a 60° C oven to remove moisture. Sediment (7.5 to 10.0 mg) was weighed into a tin capsule, and an aliquot of vanadium pentoxide in stoichiometric excess was added to drive sulfur combustion to completion. An auto-sampler delivered each sample sequentially to a combustion chamber, which was kept at 900-1000° C, driving combustion to completion. Once the sample was combusted, ultra high purity helium gas delivered SO₂, NO₂, and CO₂ to a GC column for separation and determination of sulfur, nitrogen, and carbon concentrations using a thermal conductivity detector.

Sediment subsamples for MeHg and THg were removed from the original sample container before all other analytes and placed in trace-metal cleaned glass scintillation vials in an oxygen-free atmosphere using a Teflon policeman that had been washed in 10% nitric acid. Samples were placed in a freezer (-20° C) within 10 min of sub-sampling sediment core sections. Before analysis, the sediment was freeze dried at the lab in which it was being analyzed (Mitchell, University of Toronto-Scarborough). Isotope dilution was used by spiking each sediment sample with a MeHg¹⁹⁹ as an internal standard (Hintelmann and Evans 1997; Mitchell and Gilmour 2008^b). MeHg was extracted in PTFE vessels using deionized water, KCl, and H₂SO₄ (Horvat et al. 1993). The distillate was then ethylated, volatilized, and delivered to a Tenax trap where mercury species were concentrated (Horvat et al. 1993). The Tenax trap was then heated in a stream of Hg-free argon flowing into a GC column, followed by quantification on a ICP-MS (Perkin-Elmer Elan DRC II) (Mitchell and Gilmour 2008^b). The method above

was performed by the University of Toronto as outlined by Mitchell and Gilmour (2008^b), Hintelmann and Evans (1997), Hintelmann and Ogrinic (2003), and Horvat et al. (1993). THg in sediment samples were extracted with heated H₂SO₄/HNO₃ digestions followed by dilution of the extract in deionized water (Mitchell and Gilmour, 2008^b). The sediment extract was analyzed using an ICP-MS coupled with a Perkin Elmer flow injection autosampler (Mitchell and Gilmour, 2008^b). Initial site characterization mercury samples were sent to the lab of Steve Balogh (Metropolitan Council Environmental Services). For THg extraction, 8 mL 1M HNO₃ was added to a known mass of sediment, sonicated for 15 min at 55° C, and then centrifuged for 5 min at 3000 rpm (Hammersmidt, 2001). EPA Method 1630 was used to determination THg concentrations in sediment extracts.

SRB abundance was characterized using quantitative real time polymerase chain reaction (qPCR). A MoBio PowerSoil extraction kit was used to extract total DNA from sediment samples. Using a stainless steel spatula (cleaned with acetone, 10% HCl, and Millipore water), a 0.25 to 0.3 g aliquot of sediment was placed in a PowerBead tube. DNA was extracted according to the instructions provided with the MoBio PowerSoil extraction kit. Quantitative PCR was used to estimate the abundance of sulfate-reducing bacteria by quantifying copies of the *dsrA* gene as outlined in Schippers et al. (2006) and modified by Oster (2012).

Chapter 3. Initial Condition Site Characterization

Chapter Summary

Previous research has shown that sediment methyl mercury production and transport are related to site bulk geochemistry including THg, organic carbon, AVS, DOC, and porewater sulfide. The results and discussion presented in this chapter compare the bulk geochemical parameters in characteristically different sediment types in the St. Louis River estuary, which highlight in-situ factors influencing the production of methylmercury. In addition to this spatial comparison, the following chapter will compare the response of each habitat zone to sulfate amendments.

Solid Phase Carbon Concentration and Recalcitrance

The SB habitat zone had the highest sediment %TC (4.1 to 5.6) compared with the UEF (2.1 to 3.5 %TC) and LEF (2.7 to 4.3 %TC) habitat zones. In addition to overall carbon abundance, down core trends were markedly different among the UEF, LEF, and SB habitat zones (Figure 6a). Vertical lines in Figures Figure 6, Figure 8, Figure 9, Figure 14, and Figure 15 represent the sample depth interval. In the UEF and SB habitat zones %TC decreased with depth in the sediment profile (Figure 6a), which is characteristic of the degradation of organic carbon with increasing depth over time in a depositional system (Meyers et al. 1993). Unlike the SB and UEF habitat zones, there was no discernible %TC trend with depth in the LEF habitat zone (Figure 6a). Since results from the preliminary site characterization

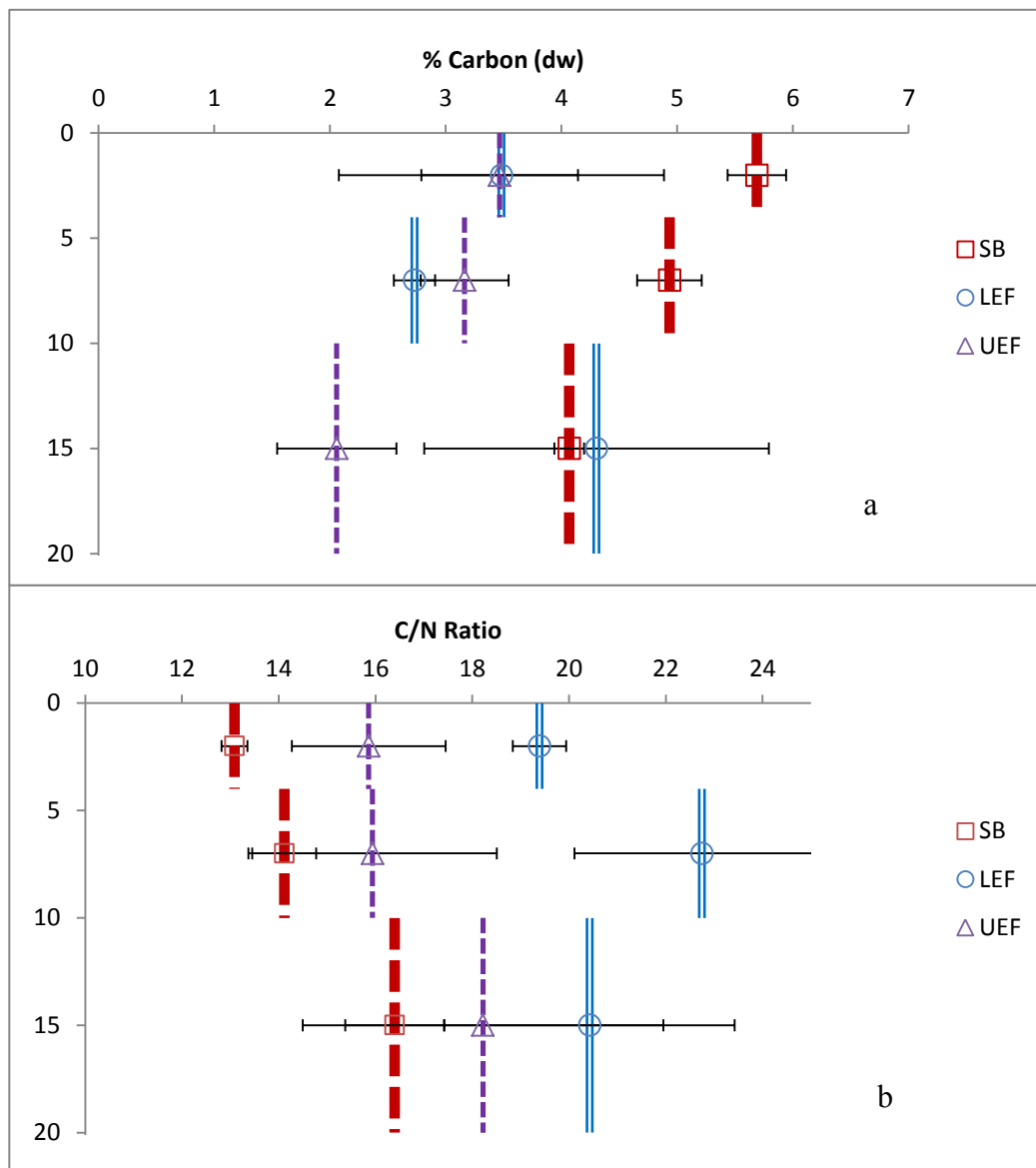


Figure 6. Initial (0 months) solid phase (a) total carbon (TC) and (b) C/N ratio. Concentrations depicted represent averages (n=3) for each depth section. Horizontal bars represent the standard deviation of the three initial sediment microcosms from each habitat zone. Vertical bars represent the length of section that each data point represents.

indicated that inorganic carbon represented less than 10% of solid phase total carbon pool, %TC herein will represent organic carbon (Figure S2).

A measure of the recalcitrance of solid phase organic carbon is the C:N ratio, which has been used as a proxy to predict methylation rates in sediment systems (Kim et al. 2011). C:N ratios between 6 and 11 have been observed for freshly produced particulate organic carbon (POC) in lake systems (Liu et al. 2007). In the St. Louis River estuary, the SB habitat zone contained a lower C:N ratio (C:N = 13.1-15.0) compared to the UEF (C:N = 15.9-18.2) and LEF (C:N = 19.4-22.7) habitat zones. The C:N ratios in the SB were slightly greater than that of newly produced organic carbon, but suggested that some labile organic carbon was present.

Labile organic carbon in the uppermost sediments is readily available for diagenetic alteration and tends to degrade most quickly under oxic conditions (Burdige 2007). The C/N ratio in the SB habitat zone (Figure 6b) suggested that microbial alteration increases the recalcitrance of organic carbon with increasing depth. This same trend was observed in sediment from the UEF habitat zone, though more variability was observed (Figure 6b). The C:N ratio between 0 and 10 cm was much higher in the LEF habitat zone suggesting that carbon supplied to the LEF sediments was more recalcitrant than the organic carbon deposited in SB and UEF habitat zone sediments (Figure 6b). Additionally, sediment C/N ratio did not increase with depth at the LEF habitat zone,

which suggested that the carbon supplied to the LEF habitat zone does not undergo major alteration after deposition, possibly due to its initial recalcitrance.

Initial Porewater Redox Results

Sediment redox porewater profiles for oxygen (O_2) and the reduced byproducts of microbial metabolism – manganese (Mn^{2+}), ferrous iron (Fe^{2+}), and sulfide (ΣS^{2-}) – were measured at four different time points (0 months, 2 months, 4 months, and 6 months) for each sediment microcosm (Figure 7, Figure S3, Figure S4, and Figure S5). Initially, oxygen was consumed within the top 2 to 5 mm in all sediment microcosms (Figure 7). The LEF habitat zone consistently exhibited porewater redox profiles characterized by high initial Mn^{2+} concentrations and no detectable Fe^{2+} and S^{2-} (Fe^{2+} and S^{2-} detection limit 40 μM and 3 μM , respectively) (Figure 7; panels a, b, and c). Mn^{2+} reached a maximum concentration of $\sim 250 \mu M$ in most cores between 2 to 8 cm and either decreased after 8 cm or was constant with depth. Observations in the UEF habitat zone for porewater constituents were nearly identical to the LEF microcosms with respect to ΣS^{2-} , Fe^{2+} , and Mn^{2+} concentrations (Figure 7; panels d, e, and f).

The constituents present in porewater of the SB habitat zone, however, were different from the LEF and UEF habitat zones. The initial time point exhibited detectable porewater iron below 5-10 cm, with low concentrations of manganese (Figure 7; panels g, h, and i). A larger quantity of labile organic carbon in the SB habitat zone may be driving greater diagenetic activity relative to the other habitat zones, and resulting in elevated iron porewater concentrations in the cores collected from this site. Ferrous iron

may be present in the UEF and LEF porewaters at depths greater than 10 to 20 cm, but this was beyond the reach of the employed sampling and analytical methods. This

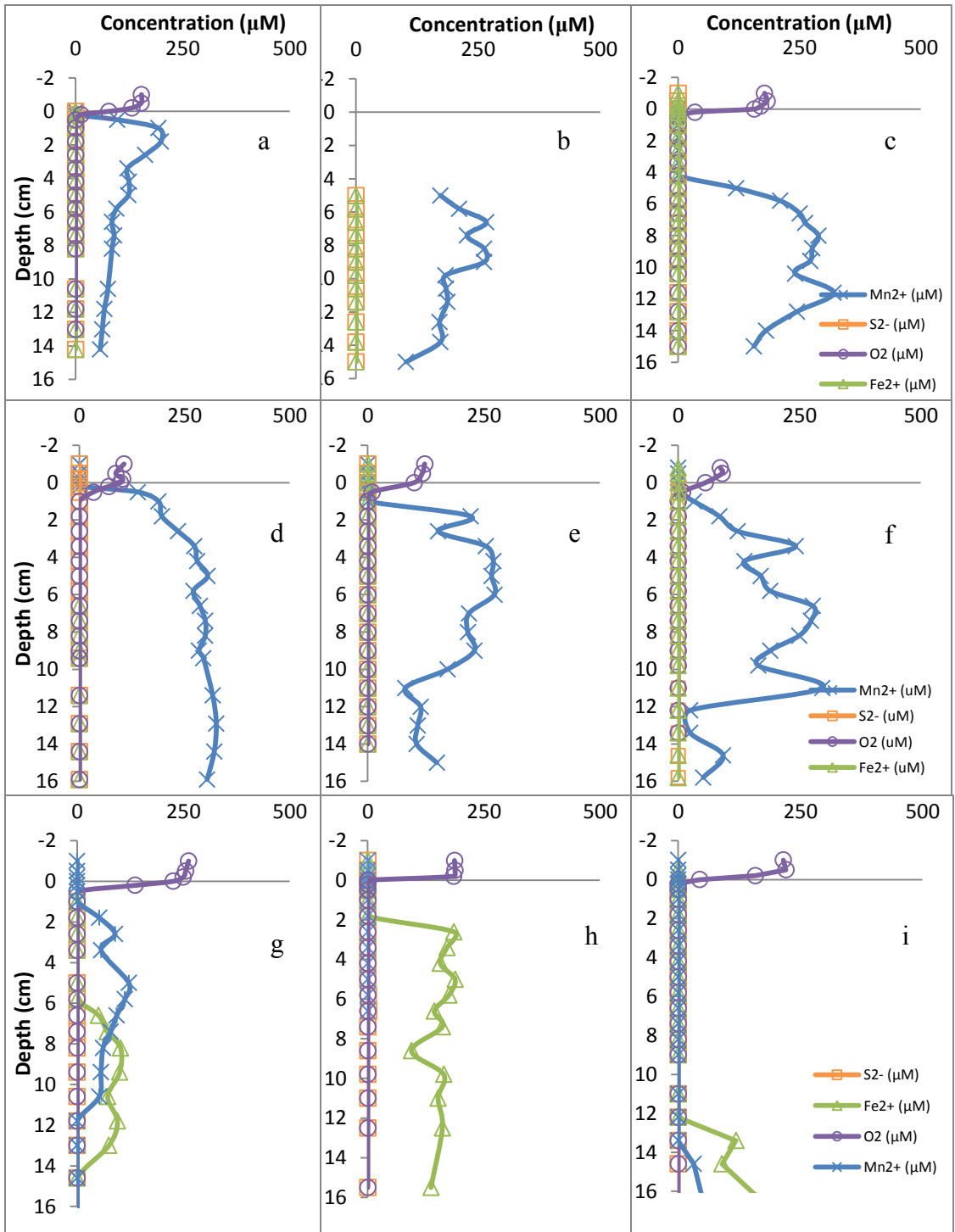


Figure 7. Initial porewater redox profiles for the LEF ((a)low, (b) control, (c) high), UEF ((d) low, (e)control, and (f)high), and SB ((g)low, (h) control, and (i)high) microcosms. A solid black line (0 cm) denotes the sediment water interface on each sediment profile.

evidence suggests that the quality and quantity of organic carbon (Figure 6) in the SB habitat zone compared to the LEF and UEF habitat zones resulted in differing porewater geochemistry and potentially different dominant microbial populations in surficial sediment

Solid Phase Acid Volatile Sulfide and Total Sulfur Results

Initial conditions indicated that SB habitat zone sediment had the greatest abundance of solid phase acid volatile sulfides (AVS) (Figure 8a). AVS concentrations in the SB sediment decreased with depth (42 $\mu\text{mol/g dw}$ at 0 to 4 cm, 8 $\mu\text{mol/g dw}$ at 10 to 20 cm). The UEF and LEF sediment had lower AVS concentrations near the SWI (1.88 $\mu\text{mol/g dw}$ and 0.22 $\mu\text{mol/g dw}$ at 0 to 4 cm, respectively) and increased to 10 to 15 $\mu\text{mol/g dw}$ with depth (Figure 8a). Although sulfide was not observed in sediment pore waters, initial AVS concentrations suggested that sulfate was being reduced rapidly in surficial sediment (0 to 4 cm) of the SB habitat zone compared to the UEF and LEF habitat zones (Figure 8a). Higher abundance of labile organic carbon in SB sediment (Figure 6) and the possibility of oxygen depletion in overlying water at the SB habitat zone (backwater, slow moving area) could be driving this difference (Figure 7 and Figure 8). Since AVS measures the least recalcitrant pool of solid phase iron sulfide minerals (FeS) (Hammersmidt and Burton 2010), total sulfur (TS) was also measured in the solid phase. Sediment from the SB habitat zone also had the largest pool of total sulfur in the solid phase (Figure 8b).

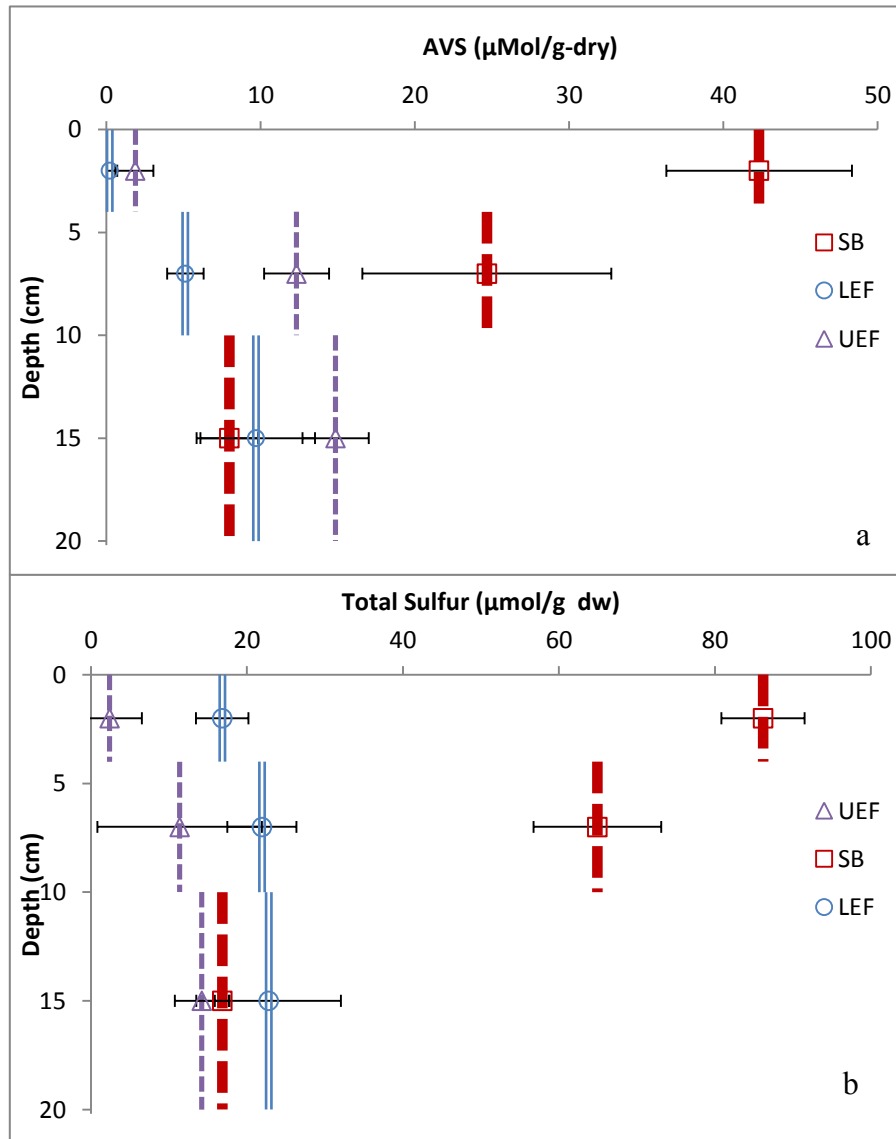


Figure 8 . Initial (0 months) (a) solid phase Acid Volatile Sulfides (AVS) and (b) Total Sulfur (TS). Values depicted represent averages (n=3) for each depth section. Horizontal bars represent the standard deviation of the three initial sediment microcosms from each habitat zone. Vertical bars represent the length of section that each data point represents

Initial MeHg/THg Results

There were clear differences in solid phase total mercury (THg) concentrations among the habitat zones sampled, with the SB habitat zone having the highest THg sediment concentration (209.4 to 358.7 ng/g). The LEF and UEF habitat zones had lower THg concentrations 74.0 to 174.6 ng/g and 52.53 to 95.35 ng/g, respectively, possibly due to lower abundance of organic carbon (Hammerschmidt and Fitzgerald, 2004^a). Sediment solid phase THg concentrations were similar to the preliminary site characterization in the LEF and SB habitat zones (Figure 9a and Figure S2f).

MeHg and THg concentrations are typically closely related in sediments with concentrations lower than 500 ng/g THg (Benoit et al., 2003), which was observed in this study (Figure 10). MeHg concentrations in sediment from the SB habitat zone were larger than those of the other habitat zones at all depths (Figure 9). Since solid phase THg concentrations varied among different habitat zones, normalization of the MeHg data was necessary to compare the capacity to produce methyl mercury between habitat zones. Fraction methyl mercury (%MeHg) in the solid phase is a unit commonly employed to determine a sediment's capacity to methylate mercury given the total inorganic mercury pool (Drott et al. 2008; Mitchell et al. 2008^b). Since %MeHg is an indicator of a sediment's capacity to methylate mercury, it was used exclusively to compare factors influencing the production of MeHg.

Despite evidence that sediment from the SB habitat zone may have had a higher abundance of sulfate reducers present in surficial sediment (0 to 4 cm) (Figure 8), the UEF

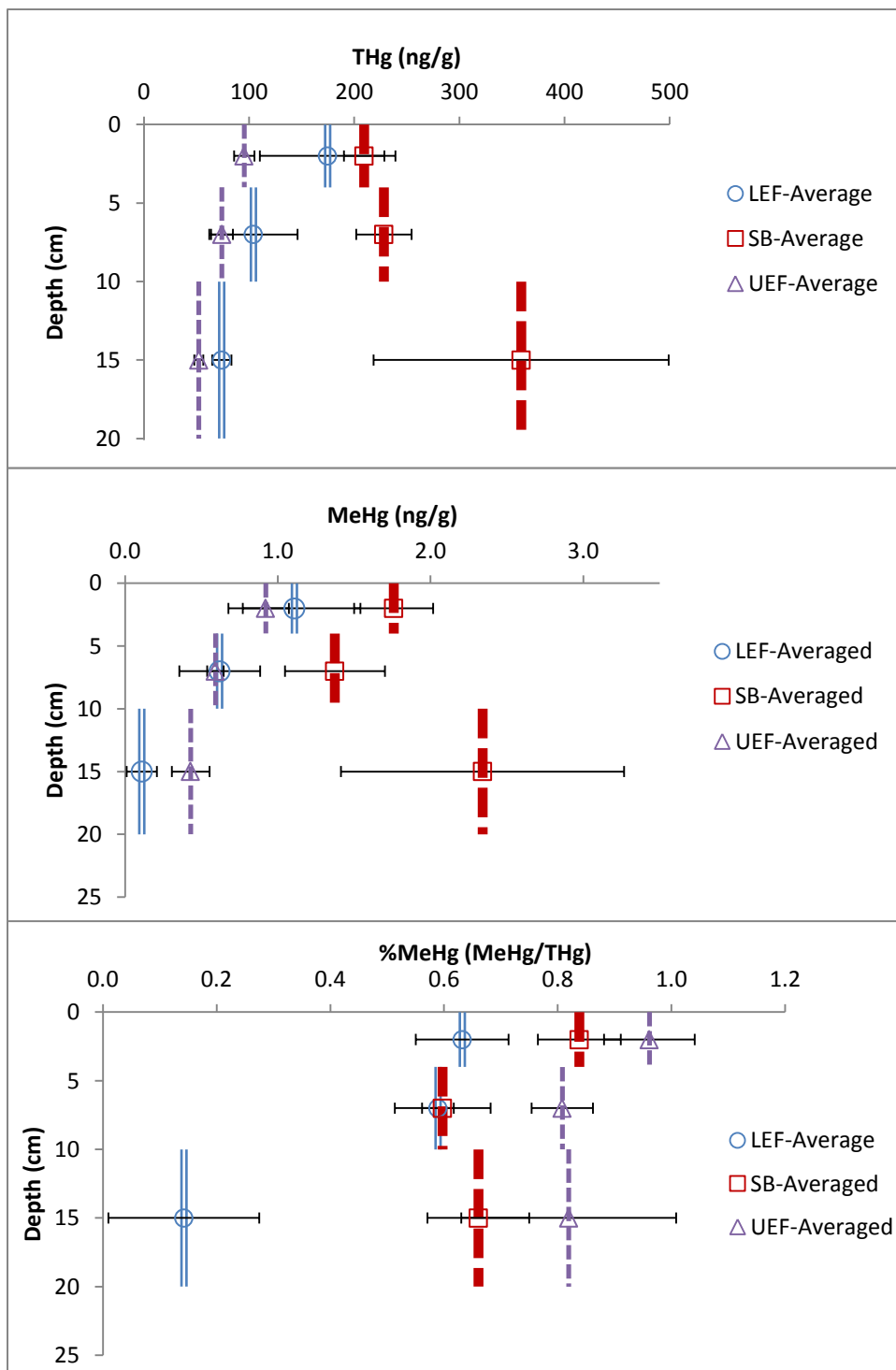


Figure 9. Initial (0 months) solid phase (a) Total Mercury (THg), (b) Methylmercury (MeHg), and (c) percent methylmercury (%MeHg). Values depicted represent averages (n=3) for each depth section. Horizontal bars represent the standard deviation of the three initial sediment microcosms from each habitat zone. Vertical bars represent the length of section that each data point represents.

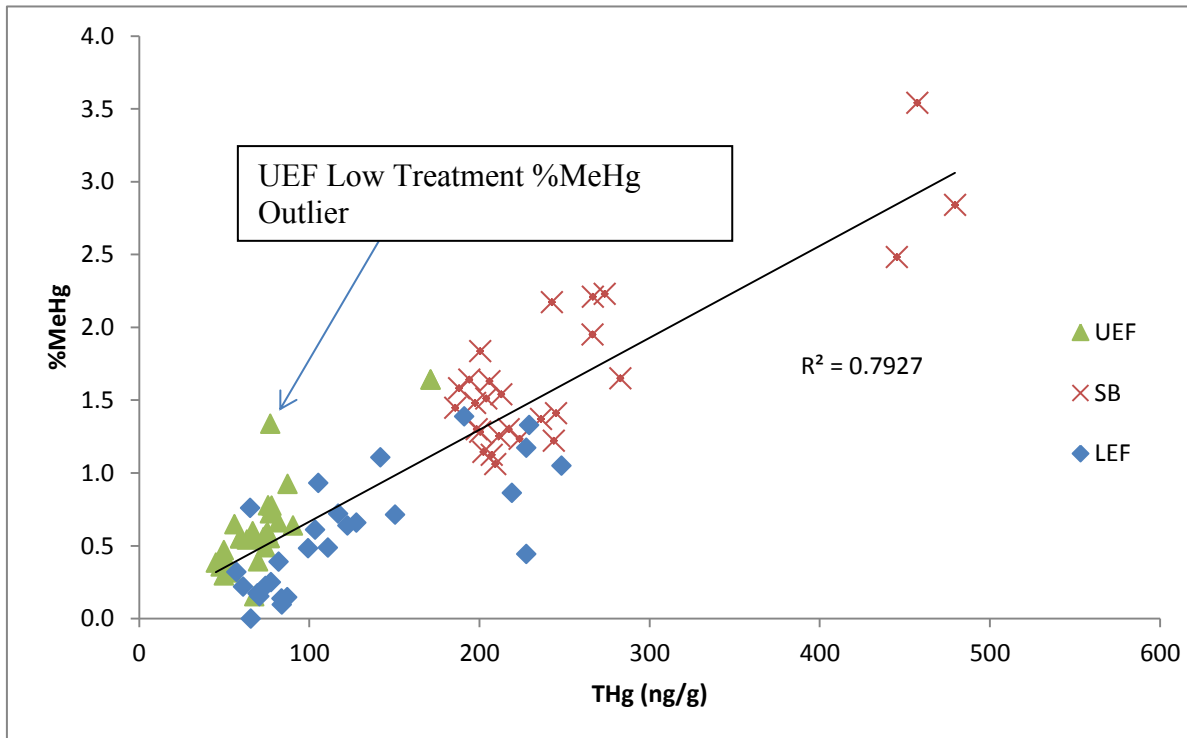


Figure 10. Relationship between solid phase THg and MeHg for the LEF (diamonds), UEF (triangles), and SB (crosses) habitat zones. R^2 value is labeled next to regression line.

habitat zone had the largest %MeHg in the top 4 cm values of the three habitat zones sampled (Figure 9c). The SB, UEF, and LEF habitat zones had %MeHg ranges of 0.60 to 0.84, 0.82 to 0.96, and 0.14 to 0.63, respectively. These data suggest that of the three habitat zones, the UEF and SB habitat zone methylate mercury most efficiently, although high total mercury in SB sediment resulted in higher absolute MeHg concentrations on the solid phase.

Porewater Mercury Partitioning

Partitioning coefficients for MeHg and THg were calculated in each habitat zone using Equation 1, where K_D [L/kg] is the solid-liquid partition coefficient, $C_{\text{porewater}}$ is the concentration in the porewater (ng/L, 0 to 10cm composite), and C_{sediment} is the concentration in the solid phase (ng/kg) at the close of the experiments. Partition coefficients therefore represent the ratio of sediment mercury to porewater mercury averaged over the top 10 cm of the microcosms. Because no discernible MeHg or THg trend was observed among experimental sulfate treatments in each habitat zone (Table S3 and Table S4), K_D values were averaged for the three microcosms in each habitat zone. For THg, the UEF and LEF had the lowest partition coefficient of 3.81 ± 0.21 and 3.88 ± 0.20 , respectively, while the SB had the largest partition coefficient of 4.70 ± 0.20 (Table 2, average ($n = 3$) \pm SD).

$$1. \quad K_D = \frac{C_{\text{sediment}}}{C_{\text{porewater}}}$$

Two bulk geochemical characteristics that differed among habitat zones were AVS and organic carbon (Hammershmidt et al. 2004^a; Turner et al. 2001; Bower et al.

Table 2. Partition Coefficients (K_D) tabulated for THg in the top 10 cm of each habitat zone.

Habitat Zone	Porewater THg (ng L ⁻¹)	Solid Phase THg (ng g ⁻¹)	THg log(K_D) [L/kg]
UEF	12.27±5.37	75.25±5.88	3.81±0.21
SB	4.48±1.80	209.77±7.87	4.70±0.20
LEF	26.29±21.63	176.2±82.99	3.88±0.20

Table 3 Partition coefficients (K_D) tabulated for MeHg in the top 10 cm of each habitat zone.

Habitat Zone	Porewater MeHg (ng L ⁻¹)	Solid Phase MeHg (ng g ⁻¹)	MeHg Log(K_D) [L/kg]
UEF	0.33±0.07	0.52±0.02	3.20±0.07
SB	0.32±0.04	1.42±0.18	3.65±0.18
LEF	0.46±0.55	0.64±0.26	3.36±0.41

2008). TC and AVS tend to be positively correlated with mercury partition coefficients since THg adsorbs strongly to organic matter and can form insoluble sulfide minerals. The SB habitat zone sediment had high concentrations of both carbon and AVS that may have increased solid phase partitioning relative to the UEF and LEF sediment (Figure 11). Strong partitioning to the solid phase in the presence of carbon and solid phase sulfides has been shown to lower the dissolved inorganic mercury available to SRB in sediments (Hammersmidt et al. 2004^a; Turner et al. 2001).

THg partition coefficients in the habitat zones sampled were comparable in magnitude relative to those measured in other estuary systems (Hammersmidt et al. 2004^a). A relationship was observed between %TC and THg partition coefficients in the St. Louis River estuary sediments (Figure 11), similar to that observed by Hammersmidt et al (2004^a), which suggests that solid phase AVS and carbon may influence mercury partitioning. In the results presented here, AVS and TC concentrations were covariate in their relationship with THg partitioning, but the limited data available for the LEF and UEF habitat zones were used to interpret the factor that had the strongest influence on dissolved THg concentrations. Although the UEF and LEF habitat zones had similar %TC (3.2% and 3.1%, respectively) in surficial sediment, they possessed markedly different AVS concentrations (8.7 and 2.7, respectively) (Figure 11). If iron sulfides did act as important adsorption or deposition sites for Hg, UEF habitat zone partition coefficients would be larger than those of the LEF habitat zone.

Organic carbon and solid phase iron sulfides also bind MeHg strongly (Miller 2006) and may control the partitioning of MeHg to the solid phase; however, MeHg

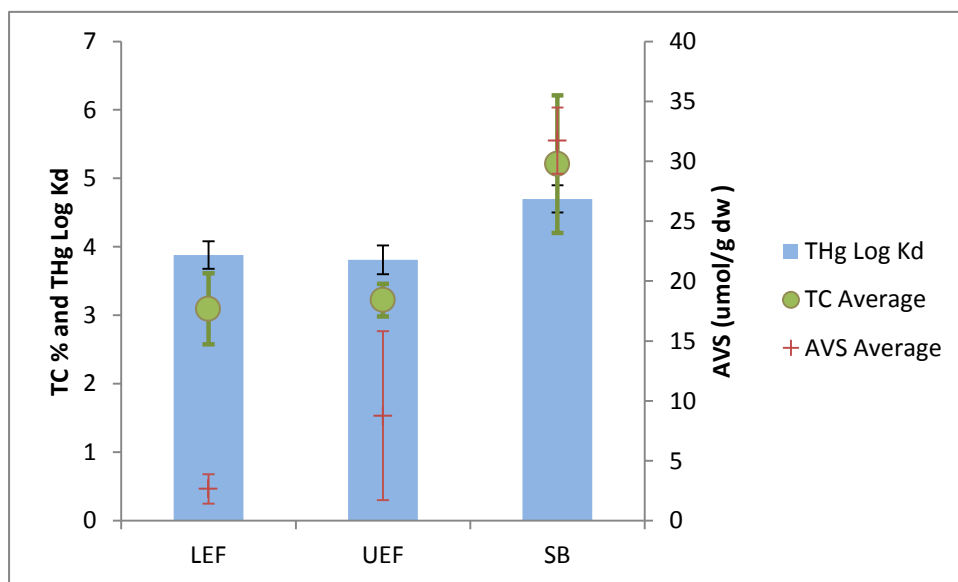


Figure 11 Average THg partition coefficients and volume weighted average TC and AVS values from the top 10 cm of each sediment microcosm. This figure depicts the influence that AVS and TC have on THg partition coefficients.

partitioning coefficients did not exhibit strong relationships to AVS or %TC (UEF (3.2±0.1), SB (3.7±0.2), and LEF (3.4±0.4) habitat zones) (Table 3). In addition, MeHg partition coefficients measured in sediments from the St. Louis River estuary were higher than most reported in the literature for marine environments (Hammerschmidt et al 2004^a, Fitzgerald et al 2007).

Discussion

Results from the initial characterization of sediment microcosms demonstrated that the three habitat zones were different with respect to both porewater (ΣS^{2-} , Fe^{2+} , and Mn^{2+}) and solid phase (C/N ratio, AVS, THg, and MeHg) characteristics. The SB habitat zone had the highest concentration and most labile organic carbon of the three sites (Figure 6). The UEF and LEF sediments had similar %TC, but the UEF sediment contained more labile organic carbon as characterized by C:N ratios. These results suggest that the SB habitat zone could drive higher diagenetic activity, and potentially biologic methyl mercury production, due to a larger abundance of labile electron donors.

AVS and dissolved biproducts of microbial metabolism (ΣS^{2-} , Fe^{2+} , and Mn^{2+}) also indicated the SB habitat zone had greater diagenetic activity in surficial sediment (0 to 4 cm). AVS concentrations in the SB habitat zone were 20 to 40 times greater than the UEF and LEF habitat zones in the top 4 cm. Labile organic carbon in the SB habitat zone was likely driving greater sulfate reduction and, thus, resulting in greater accumulation of solid phase sulfides. The UEF and LEF sediment had detectible Mn^{2+} in their

porewaters, while the SB sediment porewaters had higher concentrations of dissolved Fe^{2+} , which suggests more rapid consumption of electron acceptors.

Observations of %MeHg demonstrated that factors other than overall diagenetic activity influenced MeHg production, however. The UEF habitat zone had the highest %MeHg in the surficial sediment (0 to 4 cm) among the three habitat zones even though it had less total- and labile- organic carbon than the SB habitat zone. This result may be due to the amount of inorganic mercury available to SRB in the porewater. Sediment from the SB habitat zone had the lowest dissolved THg porewater concentrations, which would limit the amount of dissolved inorganic mercury available to SRB. Sediment from the UEF and LEF habitat zones had porewater THg that was three and six times greater than that of the SB sediments (Table 2) likely due to fewer binding sites associated with solid phase TC and AVS. In summary, the UEF habitat zone had geochemical parameters including porewater THg, organic carbon quality, and organic carbon quantity that were conducive to the production of methylmercury. Low porewater inorganic mercury may have led to less efficient MeHg production in SB sediment, while recalcitrant organic carbon may have led to less efficient MeHg production in LEF sediment.

Chapter 4 Experimental Sulfate Addition Results and Discussion

Chapter Summary

In addition to comparing mercury-related in-situ geochemical characteristics among habitat zones, the influence of overlying water sulfate concentrations on sediment methylmercury was investigated by imposing an artificial gradient of overlying water sulfate (5-50 mg/L) in a laboratory setting. Previous studies have shown that sulfate additions can enhance mercury methylation in low sulfate systems (Gilmour et. al. 1992; Jeremiason et. al. 2006). To investigate how overlying water sulfate concentrations affect mercury methylation in the intact structure of sediment from the sulfate-impacted St. Louis River estuary, measurements of sediment methyl mercury will be presented in the context of sulfate transport, SRB abundance, and AVS accumulation.

Experimental Sulfate Loading Results

Sulfate porewater concentrations were measured initially and 6 months into lab incubations. A rapid decrease in porewater sulfate from the surface water interface to 5-10 cm of sediment was indicative of biological reduction of sulfate in sediments of all habitat zones. To quantitatively compare the influence of the three overlying water sulfate treatments on the sediment column, sulfate flux was estimated using Equation 2 where F is the flux ($\text{mg cm}^{-2} \text{s}^{-1}$), D is the diffusion coefficient of sulfate in water ($5.6 \times 10^{-6} \text{ cm}^2 \text{s}^{-1}$) (Krom et al. 1980), δC is the concentration difference (mg cm^{-3}), δx is the distance (cm) over which a concentration difference is observed, θ is the tortuosity (dimensionless), and ϕ is the porosity ($\text{cm}^3 \text{cm}^{-3}$) (Boudreau 1996). Equation 3 was used to calculate the tortuosity using porosity estimates derived from wet to dry mass ratios and estimates of particle density (Boudreau 1996). Equation 4 was used to

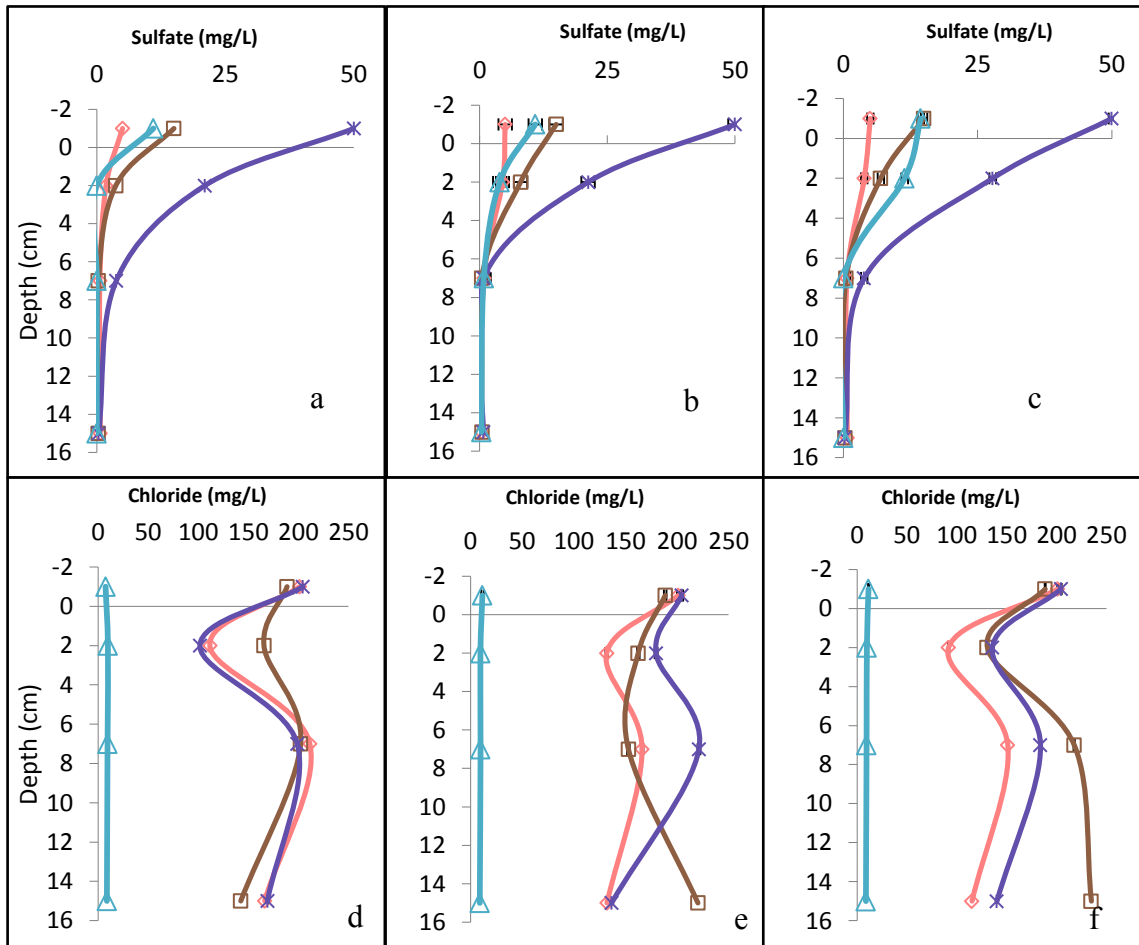


Figure 12 Sulfate and chloride porewater concentrations for (a and d) SB, (b and e) UEF, and (c and f) LEF habitat zones including overlying water concentrations for high (purple stars), low (pink diamonds), control (brown squares), and initial profiles (blue triangles). A solid black line (0 cm) denotes the sediment water interface on each sediment profile. Horizontal bars represent the standard deviation of the three initial sediment microcosms from each habitat zone.

$$2. \quad F = \frac{\varphi D}{\theta^2} \frac{\delta C}{\delta x}$$

$$3. \quad \theta^2 = \frac{1}{\varphi^2}$$

$$4. \quad D_w = (4.655 + 0.2125T) \cdot 10^{-6} \text{ cm}^2 \text{ s}^{-2}$$

calculate the diffusion coefficient of sulfate in water where D_w ($\text{cm}^2 \text{ s}^{-1}$) is the diffusion coefficient in water and T is temperature of sediment porewater ($^{\circ} \text{C}$)(Schulz 2000). δx was defined as the distance 2 cm above the SWI to the depth at which sulfate concentrations were near the analytical detection limit.

For all habitat zones, sulfate flux into the sediment was greater in the high sulfate treatments relative to the control treatments and low treatments (Figure 13). Over the 6-month experimental period, different sulfate treatments were clearly delivering variable amounts of sulfate at depths up to 7 cm in each habitat zone (Figure 12a-c and Figure 13). To track diffusional transport from the overlying water into the sediment, chloride was added as a conservative ion tracer to the overlying water treatments (200 mg/L chloride as sodium chloride). The initial porewater chloride concentrations were consistent at all depths among all sediment microcosms (7.5 to 11.5 mg/L). Chloride from the overlying treatments had diffused to the bottom of each sediment microcosm in all treatments after 6 months (Figure 12d-f) indicating that diffusion of amended solutes (chloride and sulfate) occurred in all sediment microcosms due to the overlying water treatments.

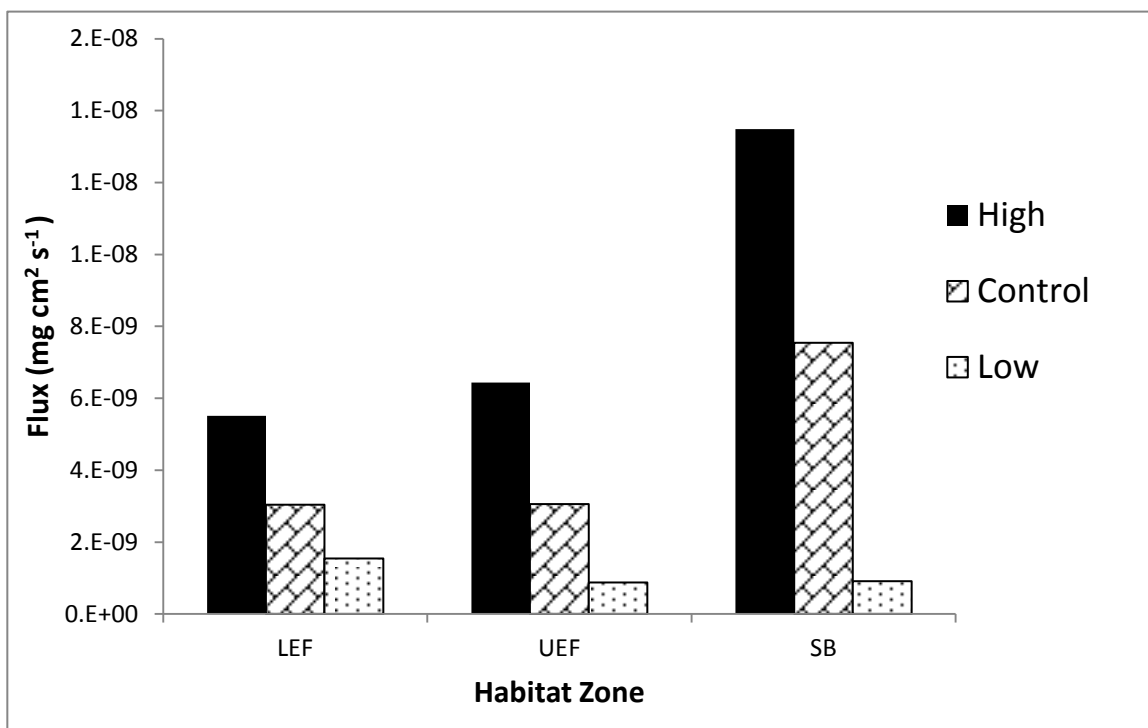


Figure 13 Estimated sulfate flux into each sediment microcosm sulfate treatment. Flux values were calculated assuming sediment particle density for LEF, UEF, and SB of 2.5, 2.0, and 1.5 g cm^{-3} , respectively.

Sulfate Reduction Indicators: SRB Abundance and AVS experimental Results

SRB abundance was measured at the initial and final time points to determine if overlying water sulfate concentrations influenced SRB metabolism in the underlying sediment (Figure 14). In the UEF and SB habitat zones, high sulfate overlying water treatments SRB abundance increased relative to initial conditions in the top 0 to 10 cm (Figure 14a and Figure 14b). Though a similar increase was noted in the control treatments, this suggests that the addition of sulfate to the overlying water stimulated the activity of SRB in surficial sediment of SB and UEF sediment (Figure 14, panels a and b). SRB abundance was not stimulated by high sulfate treatment in the LEF habitat zone (Figure 14c), however; and in fact decreased after 6 months, though the decrease was not statistically significant. In the LEF habitat zone, decreased SRB abundance in the sediment underlying the high overlying water sulfate treatment could have been a result of a limited supply of labile carbon (Figure 14c).

For the low overlying water sulfate amendments, a decrease in SRB abundance, relative to the initial conditions, in the SB and LEF low overlying water sulfate from 0 to 10 cm, suggested that decreasing sulfate concentrations in these habitat zones influenced SRB metabolism. These results suggested that lowering overlying water sulfate concentrations influenced the microbial population known for methylmercury production in sediments (0 to 10 cm) in two of the three habitat zones studied.

In addition to SRB abundance, AVS was measured in an attempt to quantify the cumulative impact of sulfate treatments in each habitat zone. The most striking observation in AVS during the 6 month experiments was a large decrease relative to

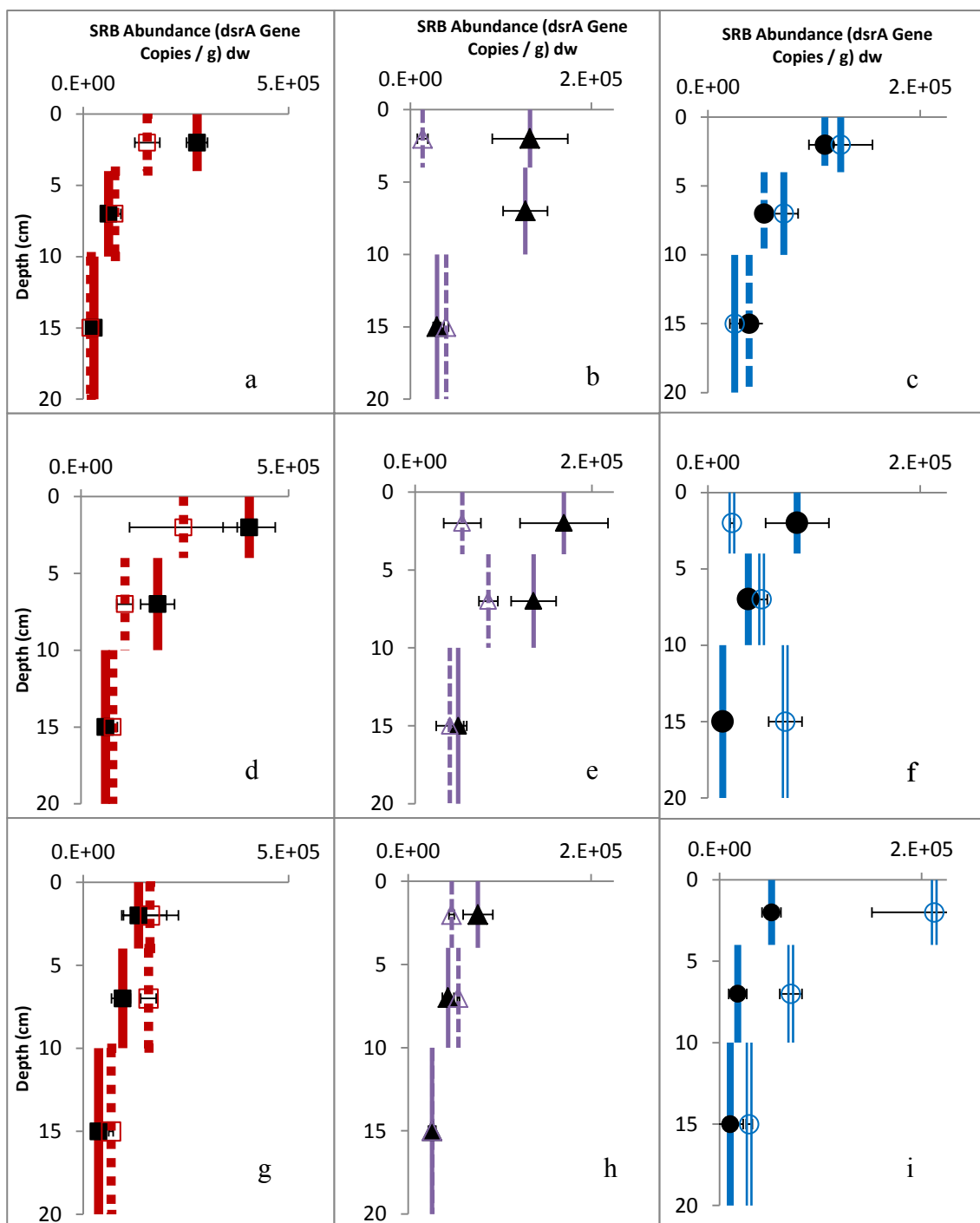


Figure 14. SRB abundance at initial (empty markers; 0 months) and final (black markers; 6 months) laboratory conditions for sediment from (a-high sulfate, d-control sulfate, and g-low sulfate) SB microcosms, (b-high sulfate, e-control sulfate, and h-low sulfate) UEF microcosms, and (c-high sulfate, f-control sulfate, and i-low sulfate) LEF microcosms. Values depicted represent averages ($n=3$) from triplicate analysis. Horizontal bars represent the standard deviation from triplicate analysis of the DNA extract. Vertical bars represent the composited interval represented by each data point.

initial conditions in AVS for all SB microcosms from 0 to 4 cm. This observation suggested that the experimental conditions altered the upper boundary condition for SB sediment, which may have been exposed to anoxic overlying water in-situ. AVS in SB and UEF microcosms increased between 4 and 10 cm in response to the high overlying water sulfate treatments relative to initial conditions; however, a similar increase was noted in the control treatments. In the LEF microcosms, AVS concentrations remained uniformly low despite significant flux of sulfate into the system, which suggests that a solid phase other than that targeted by AVS may have been accumulating reduced sulfate.

Both AVS concentrations and SRB abundance suggested that overlying water sulfate treatments influenced the SRB population in the surficial sediment (0 to 10 cm) (Figure 14 and Figure 15), though a change in redox state undoubtedly affected the SB habitat zone during the sulfate addition experiment. It should be noted that qPCR analysis is not capable of measuring SRB activity directly, but rather indicates the presence and quantity of SRB cells. However, the 6 month timescale of this experiment should have been sufficient to allow the SRB population abundance to change in response to the changes in sulfate supply from the overlying water (Hawkins and Purdy 2007). Since changes in SRB abundance and AVS concentration were related to the experimental sulfate treatments, a response in %MeHg would point towards a mechanistic connection between sediment mercury methylation and overlying water sulfate supply.

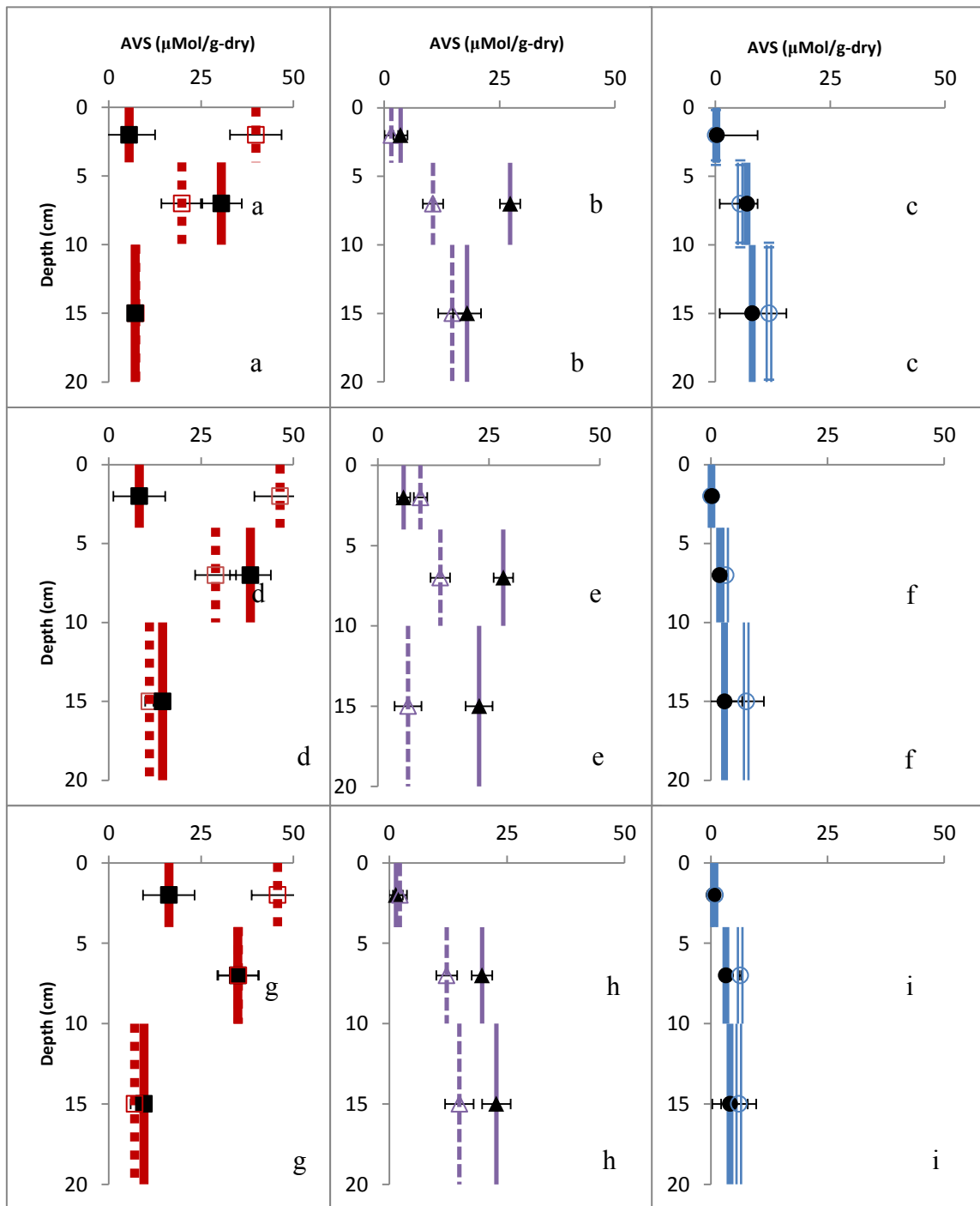


Figure 15. AVS concentrations at initial (empty markers; 0 months) and final (black markers; 6 months) laboratory conditions for sediment from (a-high sulfate, d-control sulfate, and g-low sulfate) SB microcosms, (b-high sulfate, e-control sulfate, and h-low sulfate) UEF microcosms, and (c-high sulfate, f-control sulfate, and i-low sulfate) LEF microcosms. Horizontal bars represent the standard deviation of the three initial sediment microcosms from each habitat zone. Vertical bars represent the composited interval represented by each data point.

%MeHg Experimental Results

At the end of the six-month incubation, observations of %MeHg at different depth intervals of the high, control, and low sulfate microcosms allowed an evaluation of the influence of overlying water sulfate on MeHg production in each habitat zone (Figure 16). Analyses of triplicate cores during the initial sampling were used to derive standard deviation for all sediment cores in the final time point (6 month) for statistical analysis (student t-tests). Since laboratory conditions may have altered the redox state from in-situ conditions in the SB habitat zone (regardless of sulfate amendment) the interpretation presented herein relies primarily on comparisons among sulfate treatments within a habitat zone at the end of the six month incubation (rather than a comparison of %MeHg at the end of the lab incubation to %MeHg at the beginning of the incubation).

In the surficial 0 to 4 cm section of the LEF habitat zone microcosms, %MeHg was similar in the low, control, and high sulfate treatment microcosms (%MeHg = 0.42 to 0.46) (Figure 16, panel h). Between 4 and 10 cm, however, %MeHg displayed a decreasing trend from the high sulfate to low sulfate treatment, but the differences from the control treatment were not significant (Figure 16, panel h). It should be noted that the final %MeHg results from each LEF microcosm were lower than the initial results. A possible carbon limitation may have been imposed on the LEF microcosms during the experimental period. This may have been caused by a lack of fresh organic matter being delivered to the sediment since the overlying water was recirculated continuously and refreshed only three times during the experimental period. Although there were no statistically significant %MeHg changes from the control treatment in the LEF habitat

zone, observations suggest that the overlying water sulfate treatments may have influenced the methylation and demethylation process between 4 to 10 cm. The variable (60 to 250 ng/g) total mercury present in LEF sediment resulted in absolute solid phase MeHg concentrations between 0.2 and 1 ng/g.

In the SB microcosms, %MeHg values in the surficial sediment (0 to 4 or 4 to 10 cm) did not change significantly in response to the low or high sulfate overlying water treatments when compared to the control sulfate treatment (Figure 16 panel b). Consistently high concentrations of total mercury (200 to 280 ng/g) resulted in consistent absolute MeHg concentrations between 1 and 2.2 ng/g.

In the UEF microcosms (Figure 16 panel e), there was an increase in sediment %MeHg underlying the high sulfate treatment relative to the control treatment in the 0 to 4 cm interval, though it was not significant ($p > 0.05$). Results from the UEF microcosm amended with low sulfate did show a significant decrease in sediment %MeHg ($p < 0.05$) from 4 to 10 cm at the close of the experiments, relative to the control sulfate treatment. Since AVS observations suggested that sulfate reduction was occurring from 4 to 10 cm, it is possible that decreasing the sulfate supply to the area of active sulfate reduction slowed mercury methylation at this depth interval. The depth interval of 0 to 4 cm in the low UEF microcosm displayed a significant increase relative to the control UEF microcosm. However, geochemical trend analysis (Figure 17) indicated that the 0 to 4 cm %MeHg (low UEF sulfate treatment) may be an outlier when compared to the entire data set. Because there is only one data point representing the 0 to 4 cm interval in the

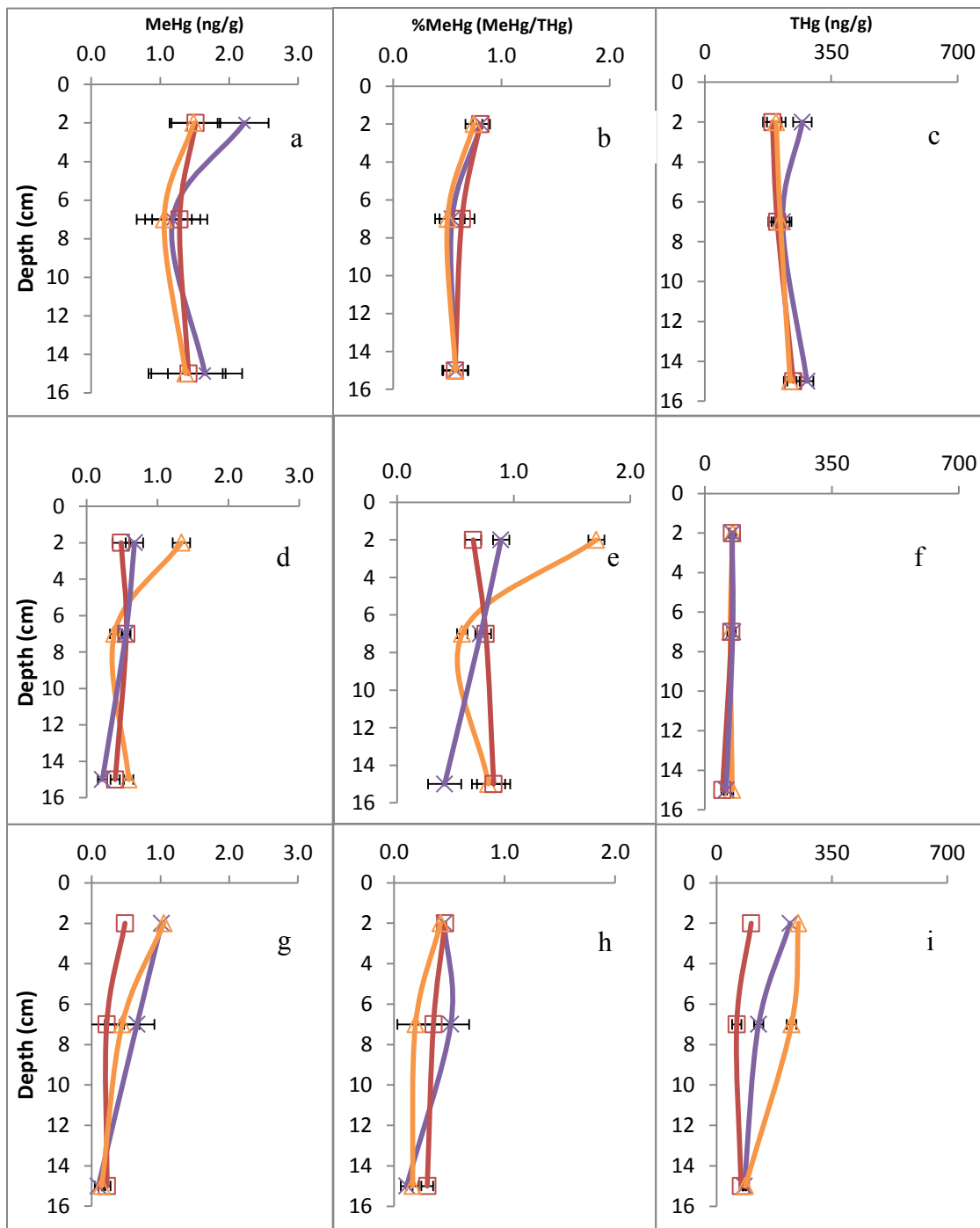


Figure 16. Solid phase MeHg, %MeHg, and THg sediment profiles for (a, b, and c) SB, (d, e, and f) UEF, and (g, h, and i) LEF habitat zones at the end of the 6-month experiment. High (purple stars), low (yellow triangles), and control (red squares) overlying water sulfate amendments. Horizontal bars represent the standard deviation of the three initial sediment microcosms from each habitat zone. Points represent samples from 0-4cm, 4-10cm, and 10-20cm intervals.

UEF low microcosm, removing this outlying data point makes it impossible to determine if the low sulfate amendment actually resulted in a significant %MeHg change. UEF sediment had consistently low total mercury (60-75 ng/g) and with the exception of the outlier, consistent absolute MeHg concentrations between 0.2 and 0.7 ng/g.

Overall, there was little variation in %MeHg (0.2 to 0.9) among sediments incubated with differing overlying water sulfate, suggesting that solid phase MeHg concentrations were not strongly influenced by overlying water sulfate concentrations. Observations did suggest that mercury methylation was significantly influenced by overlying water sulfate concentration in one instance (UEF low overlying sulfate treatment; 4 to 10 cm) and potentially correlated in another (LEF 4-10 cm). However, the trend of increased methyl mercury with higher overlying water sulfate was not consistently observed or present in surficial (0 to 4 cm) sediment of any habitat zone. Since it did appear that sediment SRB abundance and AVS concentration responded to overlying sulfate treatments in the surficial sediment of UEF and SB habitat zones, the expectation was that a concomitant response in MeHg would be observed. However, the disparity in the response of sulfate reduction indicators and %MeHg suggested that methylmercury production was not strongly influenced by overlying water sulfate, but controlled by other biogeochemical factors such as inorganic mercury bioavailability, solid phase total mercury, and organic matter quality.

Discussion

In the St. Louis River estuary, each habitat zone contained a different combination of factors influencing the production of MeHg. There was an increase in SRB abundance in the high sulfate treatments for SB (0 to 4 cm) and UEF (0 to 10 cm) sediment, indicating that SRB were stimulated by the sulfate treatment (Figure 14); however, concomitant increases in %MeHg were not observed. In addition, SRB abundance and AVS concentration decreased in the low sulfate treatments of the SB and LEF sediments indicating that a low sulfate concentration influenced the SRB in the manner expected but did not influence solid phase MeHg significantly. Although SRB are typically the primary methylators of mercury, overlying water sulfate concentration was only significantly related to %MeHg in the 4 to 10 section of the low UEF sulfate treatment (Figure 16).

The quantity and quality of carbon influenced the production of MeHg by two separate mechanisms in sediments from the St. Louis River estuary. The quality of carbon was important because a lack of labile organic carbon can reduce the production of methylmercury by suppressing the activity of SRB (Lambertsson et al. 2006). Additionally, the presence of high quantities of carbon can decrease bioavailability of inorganic mercury to SRB, and thus decrease mercury methylation (Hammersmidt et al. 2004^a). Both MeHg limiting processes may have occurred in the St. Louis River estuary sediment, depending on the habitat zone.

In the LEF habitat zone, the quality of carbon in the sediment was refractory (Figure 6), resulting in a negative correlation ($p < 0.05$) between %TC and %MeHg in the LEF system, similar to the trend observed by Hammshersmidt et al (2004) (Figure 17). Since the carbon pool in the LEF sediment was refractory, larger %TC within this site may have resulted in a larger abundance of sorption sites for inorganic mercury, but not an increase in labile electron donors. Therefore, the net effect of carbon in the LEF habitat zone appeared to be a decrease in the production of MeHg due to a combination of lowered inorganic mercury bioavailability and lack of useful electron donors (Figure 17).

In the SB and UEF habitat zones, the quality of the carbon present was labile, which stimulated microbial activity and the biological production of MeHg. There was a positive relationship between total carbon and %MeHg ($p < 0.05$) in the SB habitat zone (Figure 17). Total carbon and %MeHg also were related in the UEF habitat zone (Figure 17), but this relationship was not statistically significant ($p > 0.05$). In the SB habitat zone, higher quantities of labile carbon provide additional labile electron donors used by SRB to methylate mercury (Lambertsson et al. 2006). However, the large quantity of carbon present in SB sediment likely contributed to a very low concentration of inorganic mercury in the pore water, which may have limited mercury methylation (Figure 11 and Figure 16).

Many studies have cited a limitation of inorganic mercury to SRB due to high porewater sulfide concentrations (Benoit et al. 1999^b; Gilmour et al. 1998). In the St. Louis River estuary, sulfide concentrations were always below 3 μM , which is below the

reported threshold of sulfide limitation of MeHg production (<5-10 μM sulfide, Benoit et al. 2003). Thermodynamic calculations were not conducted for porewater mercury species but since the porewater pH was above 7 (Figure S1) and sulfide concentrations were below 5 μM , it is likely that inorganic mercury-sulfide species were uncharged, though their importance relative to organic thiol complexes is unknown (Skylberg 2008). A more detailed thermodynamic and analytical investigation would be required to elucidate porewater mercury speciation.

Collectively, the measurements and interpretations made in this study suggest that MeHg production in contrasting areas of the sulfate-impacted St. Louis River estuary were consistently related to the quantity and quality of carbon rather than overlying water sulfate concentration. Despite having a significant amount of inorganic mercury in the porewater, MeHg production in the LEF habitat zone seemed to be inhibited by a lack of labile carbon capable of driving microbial activity. The SB habitat zone sediment contained labile carbon, but low porewater THg concentrations likely limited the quantity of dissolved inorganic mercury available to drive methylation. The UEF habitat zone contained carbon that was not as recalcitrant as the LEF habitat zone and had lower solid phase carbon concentrations than the SB habitat zone. This combination of carbon quantity and quality resulted in the UEF habitat zone having the highest %MeHg in the top 4 cm, according to initial %MeHg measurements. However, all habitat zones had similar %MeHg relative to those reported in marine sediments (Fitzgerald et al 2007). Overall, it appears that the range of organic carbon quantity and quality, bioavailable inorganic mercury, and total mercury concentrations play an

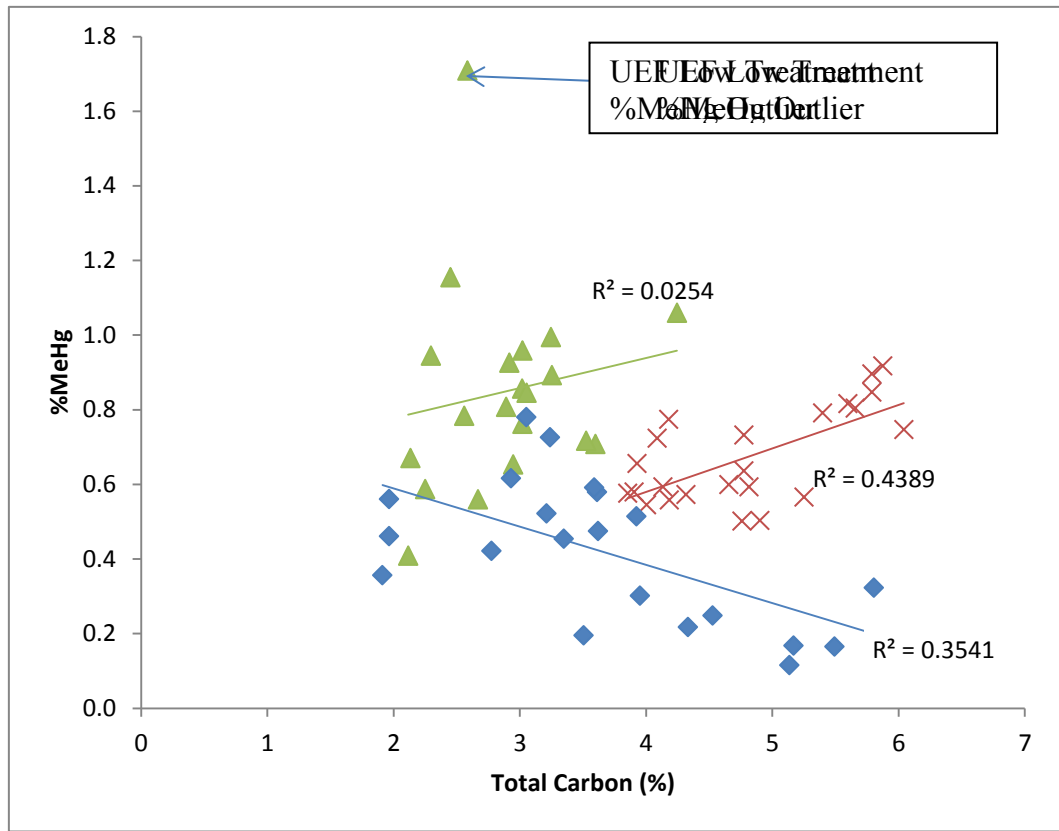


Figure 17 Relationship between % MeHg and TC Abundance for LEF (diamonds), UEF (triangles), and SB (crosses) habitat zones. Data points represent measurements made at the initial and final time points. R^2 and p values are labeled next to the regression line they represent.

important role in the production of MeHg in the sulfate-impacted St. Louis River estuary sediments.

Chapter 5 THg and MeHg Transport

In order to quantify the transport of MeHg produced in the sediments (0 to 10 cm) to the overlying water, flux measurements were made in laboratory microcosms at the close of the laboratory experiments. Laboratory flux estimates for each habitat zone were then scaled to estimate the MeHg and THg loads from sediment to overlying water in the St. Louis River estuary.

THg flux was determined by measuring the change in THg concentration in the overlying water (ΔC) of each microcosm over a 36 to 48 hour time-period (Δt). Overlying water mercury measurements were normalized to the volume of overlying water (V_w) and microcosm sediment surface area (A) to estimate flux according to Equation 5. Since THg flux had little variation among sulfate treatments, values were averaged for each habitat zone ($n = 3$).

$$5. \quad Flux_{THg} = \frac{\Delta C \cdot V_w}{\Delta t \cdot A}$$

Measurements suggested that THg flux out of the sediment was related to porewater THg concentrations. The SB habitat zone had the lowest porewater THg concentration (4.5 ng L^{-1}) as well as the lowest THg flux ($15.5 \text{ ng m}^{-2} \text{ d}^{-1}$) of the three habitat zones (Table 4 and Table 5) despite having highest THg on the solid phase (Figure 16). The LEF habitat zone had a THg flux ($40.2 \text{ ng m}^{-2} \text{ d}^{-1}$) two times greater than the UEF habitat zone ($18.5 \text{ ng m}^{-2} \text{ d}^{-1}$), which was also consistent with larger

porewater THg concentrations (Table 4 and Table 5). Measured THg fluxes from the St. Louis River estuary were within the range reported in other estuary systems, but would be considered relatively low compared to heavily contaminated systems (Choe et al. 2004; Covelli et al. 1999; Mason et al. 2006).

MeHg flux was measured in a similar manner as THg flux, but due to experimental complications and analytical resolution, MeHg flux could not be directly calculated. In place of direct measurements, estimates were made using an effective mass transfer coefficient (k_{mt}) calculated from the THg flux experimental results. Using measurements of THg flux, overlying water THg concentration, and porewater THg concentration, an effective mass transfer (effective diffusion) coefficient for THg was calculated for each habitat zone (average, $n=3$) using Equation 6. Since the overlying water and porewater MeHg concentrations were known, MeHg flux could be estimated using Equation 6, assuming the mass transfer coefficient for THg and MeHg were equal.

$$6. \quad Flux = k_{mt} (Concentration_{Porewater} - Concentration_{Overlying\ Water})$$

MeHg flux estimates were between 0.8 and 11% of measured total mercury fluxes, consistent with MeHg porewater concentrations between 1.7 and 6.6% of THg. The SB habitat zone had the largest estimated MeHg flux value ($1.75 \text{ ng m}^{-2} \text{ d}^{-1}$) as a result of having the largest k_{mt} . UEF and LEF habitat zones had lower MeHg flux estimates of 0.15 and $0.72 \text{ ng m}^{-2} \text{ d}^{-1}$, respectively. Similar to THg fluxes, estimated MeHg fluxes from the St. Louis River estuary were on the low end of a range reported in other estuary systems (Choe et al. 2004; Covelli et al. 1999; Mason et al. 2006; Hammerschmidt et al. 2008; Benoit et al 2009).

Table 4 Porewater MeHg and THg concentrations averaged in each habitat zone (n=3). Overlying water MeHg and THg concentrations from the flux experiments taken at the initial time point (t=0).

Habitat Zone	Porewater MeHg (ng L ⁻¹)	Overlying Water MeHg (ng L ⁻¹)	Porewater THg (ng L ⁻¹)	Overlying Water THg (ng L ⁻¹)
LEF	0.46±0.55	0.18±0.18	26.29±21.63	1.45±0.10
UEF	0.33±0.07	0.25±0.37	12.27±5.37	1.43±0.15
SB	0.32±0.04	0.04±0.06	4.48±1.80	1.42±0.15

Table 5 Measured THg and estimated MeHg flux for each habitat zone.

Habitat Zone	Measured THg Flux (ng m ⁻² d ⁻¹)	K _{mt} (L m ⁻² d ⁻¹)	Estimated MeHg Flux (ng m ⁻² d ⁻¹)
LEF	40.23±19.71	2.60	0.72
UEF	18.50±5.98	1.88	0.15
SB	15.47±7.94	6.14	1.75

Table 6 MeHg and THg loads estimates from each habitat zone. Loads were calculated using areas of fluxes from each habitat zone.

Habitat Zone	Area (km ²)	MeHg Load (mg d ⁻¹)	THg Load (mg d ⁻¹)
LEF	10.53	7.6	423.2
UEF	8.27	1.2	152.9
SB	3.59	6.3	55.5

Table 7 MeHg and THg concentration measured at the Scanlon Dam in Cloquet taken from Berndt and Bavin (2009). MeHg load calculated from USGS flow data obtained on the same day MeHg water sample was taken.

Site	MeHg Conc. (ng L ⁻¹)	THg Conc. (ng L ⁻¹)	Flow Rate (L d ⁻¹)	Flow exceedance (%)	Load MeHg (mg d ⁻¹)	Load THg (mg d ⁻¹)
Scanlon Dam	0.15	2.0	2.67x10 ⁹	29.5	400.0	5333.5
Scanlon Dam	0.3	6.4	2.59x10 ¹⁰	97.0	7780.1	165975.4
Scanlon Dam	0.09	2.5	1.93x10 ⁹	14.0	173.3	4813.6

Sediment fluxes were scaled to the total area of each habitat zone to obtain sediment loading estimates (mg d^{-1}) to the St. Louis River estuary (Table 6). MeHg load estimates from the LEF, UEF, and SB habitat zone sediments were 7.6, 1.2, and 6.3 mg d^{-1} , respectively, while THg load estimates totaled 632 mg d^{-1} . Upstream MeHg loading to the estuary (Table 7) was also calculated using THg and MeHg concentrations measured by Berndt and Bavin (2009 and 2012) and discharges from USGS gauge stations located at the Scanlon Dam at multiple time points (St. Louis River discharges were taken from the same day mercury water samples were obtained). The incoming MeHg load at the Scanlon Dam was calculated to be 173.3 mg d^{-1} during low flow (14% flow exceedance) conditions, 7780.1 mg d^{-1} during high flow (97% flow exceedance) conditions, and 400.0 mg d^{-1} near median flow (30% flow exceedance) conditions (Table 7). If summed, the total MeHg load from the three habitat zones (representing 45% of the total area in the St. Louis River estuary) represents 0.2 to 8.7% of the total amount of MeHg delivered to the estuary, depending on the flow regime.

Some habitat zones not included in this study contain sediments that are contaminated with respect to mercury ($>1000 \text{ ng g}^{-1}$ THg) (Crane 2006), which could result in small portions of the estuary contributing disproportionately large amounts of mercury to the overlying water column. In other contaminated sediment systems with THg concentrations greater than 1000 ng g^{-1} , sediment MeHg and THg fluxes have been reported up to three orders of magnitude greater than those measured in the LEF, UEF, or SB habitat zones. If habitat zones with high concentrations of solid phase mercury (THg) in the St. Louis River estuary have MeHg fluxes similar in magnitude to those in other

contaminated systems, sediment MeHg flux from these small, heavily contaminated areas could contribute a substantial amount of MeHg to the overlying water.

Since mercury flux was not measured in half of the estuary and in no heavily contaminated locations, it is still uncertain how important sediment is as a source of MeHg to the St. Louis River estuary. If other habitat zones contribute MeHg fluxes similar or greater to those estimated in this study, the MeHg load from sediment in the estuary could exceed 20% of total loads to the estuary during low flow conditions but will likely be overshadowed by upstream sources during high flow conditions.

Chapter 6 Conclusions and Implications

The lack of change in sediment MeHg concentration in the St. Louis River estuary observed during sulfate addition experiments coupled with the distinct differences observed among habitat zones suggests that MeHg production in surficial sediment (0 to 4 cm) depends more on organic carbon than overlying water sulfate. Only one depth interval (4 to 10 cm) of the low overlying water sulfate treatment in the UEF habitat zone experienced a statistically significant decrease in sediment %MeHg as a result of decreasing sulfate concentrations in the overlying water. Though measurements of %MeHg from 4-10 cm in the LEF habitat zone were positively related with sulfate concentrations in the overlying water, differences from the control were not significant. Carbon appeared to influence MeHg in each habitat zone depending on the quality and quantity of carbon. The UEF and SB habitat zones had similarly low C/N ratios, which may have facilitated higher microbial activity. However, lower carbon and iron sulfides

(represented as AVS) in the UEF habitat zone may have rendered more porewater inorganic mercury available for methylation relative to the SB habitat zone (Table 2).

Another important conclusion that can be drawn from the data presented is that decreasing THg in surficial sediments of the St. Louis estuary would likely result in a decrease in solid phase MeHg concentrations (Figure 10). Consistent with other studies (Benoit et al. 2003), the dataset presented here illustrates that solid phase THg and MeHg concentrations are highly correlated. In all habitat zones, there was a significant positive relationship ($p < 0.05$) between MeHg and THg, indicating that THg has a strong influence on MeHg concentrations and that methylation efficiency is not as important a factor as total mercury in determining absolute MeHg concentrations (Figure 10). While an understanding of sulfate and carbon limitations on sediment MeHg production and transport could help sulfate management decisions, decreasing atmospheric and terrestrial mercury loading to the St. Louis River estuary sediment would likely lead to a decrease in surficial sediment (0 to 4 cm) MeHg concentration.

Further investigation is needed to fully understand factors limiting MeHg production and transport in the St. Louis River estuary. Porewater and solid phase inorganic mercury speciation is frequently cited as an important factor in the production of MeHg (Graham et al. 2012; Schaefer et al. 2011; Deonaraine and Hsu-Kim 2009). Methylmercury speciation has also been suggested as an important factor in MeHg transport although detailed thermodynamic modeling of MeHg species is required (Jonsson et al. 2010; Berndt and Bavin 2011). Furthermore, determining the abundance

of FeRB in addition to SRB may determine which microbial population is the primary methylator of mercury.

MeHg fluxes were estimated for each habitat zone to quantify mass loadings to the St. Louis River estuary system. For the habitat zones examined in this study (45% of the total area of the St. Louis River Estuary), it was estimated that flux from sediment could contribute a MeHg load of 15.1 mg d^{-1} to the overlying water. Comparatively, upstream MeHg contribution to the estuary (estimated from in-stream measurements at Scanlon, MN) was 400.0 mg d^{-1} during near-median flow and 173.3 mg d^{-1} low flow conditions. Under high flow regimes, the MeHg contribution from upstream becomes two orders of magnitude larger (7780.1 mg d^{-1}) than that of the sediment. These sediment flux estimates suggest that MeHg loading from the LEF, UEF, and SB (not heavily contaminated areas) habitat zones represent a small, but not insignificant source of MeHg to the estuary water column during median and low flow conditions relative to upstream sources.

Although these flux results suggest that MeHg loading from sediment is small relative to upstream loading, only 45% of the estuary was accounted for in this study. To gain a quantitative understanding of the MeHg and THg mass balance within the St. Louis River estuary and determine if sediment from the estuary is an important source of mercury, it is necessary to measure fluxes from a larger percentage of the St. Louis River estuary, including sites with higher sediment mercury concentrations. Furthermore, determining residence times of specific regions of the estuary is needed to obtain an accurate mass balance and the relative importance of upstream MeHg loading compared

to sediment MeHg loading. For example, residence times in habitat zones located in areas with little bulk advective flow in the overlying water (SB) are likely much longer than areas near the main channel (LEF and UEF). Areas with longer overlying water residence times, such as the SB habitat zone, could receive a much larger proportion of MeHg from sediment loading.

If further study is to be done on sediment-water mercury exchange in the St. Louis River estuary, selection of an appropriate method to measure flux is paramount. Although it is possible to estimate diffusion-driven effluxes using Fick's first law of diffusion given a MeHg concentration gradient in porewater (Hammerschmidt et al. 2004^b; Gill et al. 1999), this method frequently underestimates MeHg flux (Benoit et al. 2009). In-situ benthic flux chambers can be used to measure MeHg flux from sediment and are considered the most accurate method; however, they are expensive to fabricate and maintain, require trained divers for sampling, are difficult to deploy in high traffic water bodies, (Hammerschmidt and Fitzgerald 2008) and still subject to experimental artifacts (e.g., flux chambers limit groundwater advection and likely disturb benthic organisms). Laboratory sediment core incubations are a simpler and more cost effective method for measuring MeHg flux, although it is difficult to replicate in-situ redox, light, and temperature conditions with this method.

This study addressed multiple scientific and management questions related to the production and transport of MeHg in the St. Louis River estuary. The implications of changing sulfate concentrations in the overlying water were interpreted in the context of organic carbon and other geochemical factors influencing the production of MeHg in

each habitat zone. Although it was estimated that the sediment MeHg flux from unimpacted areas comprises a small amount of MeHg to the water column relative to upstream sources, sediment could still influence the total pool of MeHg in the St. Louis River estuary, particularly in low-flow situations. Results presented have illuminated the role of sulfate and carbon in the production and transport of MeHg and begin to place sediment MeHg loading to the St. Louis River estuary in the context of upstream MeHg loads.

References

- Benoit, J.M., Gilmour C.C., Mason, R.P., Heyes, A. (1999^a). Sulfide controls on mercury speciation and bioavailability to methylating bacteria in sediment pore waters. *Environmental Science and Technology* 33(6): 951-957.
- Benoit, J.M., Mason, R.P., Gilmour, C.C. (1999^b). Estimation of mercury sulfide-speciation in sediment pore waters using octanol-water partitioning and implications for availability to methylating bacteria. *Environmental Toxicology and Chemistry* 18(10): 2138-2141.
- Benoit, J.M., Gilmour C.C., Mason, R.P. (2001). Aspects of bioavailability of mercury for methylation in pure cultures of *Desulfobulbus pronionicus* (1pr3). *Applied and Environmental Microbiology* 67(1): 51-58.
- Benoit, J.M., C.C., Gilmour, Heyes, A., Mason, R.P., Miller, C.L. (2003). Geochemical and biological controls over methylmercury production and degradation in aquatic ecosystems. *Biogeochemistry of Environmentally Important Trace Elements – ACS Symposium Series 835*: 262-297.
- Benoit, J.M., Shull, D.H., Harvey, R.M., Beal, S.A. (2009). Effect of bioirrigation on sediment-water exchange of methylmercury in Boston Harbor, Massachusetts. *Environmental Science and Technology* 43(10): 3669-3674.
- Berndt, M.E. and Bavin, T.K. (2009). Sulfate and mercury chemistry of the St. Louis River in Northeastern Minnesota. MN DNR Report, Division of Land and Minerals
- Berndt, M.E. and Bavin, T.K. (2011). Sulfate and mercury cycling in five wetlands and a lake receiving sulfate from Taconite mines in northeastern Minnesota: A Report to Iron Ore Cooperative Research Program., Minnesota Department of Natural Resources, Division of Lands and Minerals, St. Paul, MN.
- Berndt, M.E. and Bavin, T.K. (2012)^a. Methylmercury and dissolved organic carbon relationships in a wetland-rich watershed impacted by elevated sulfate from mining. *Environmental Pollution* 161:321-327
- Berndt, M.E. and Bavin, T.K. (2012)^b. On Cycling of sulfur and mercury in the St. Louis River watershed, northeastern Minnesota, Minnesota Department of Natural Resources. An Environmental Trust Fund Report.
- Boudreau, B.P. (1996). The diffusive tortuosity of fine-grained unlithified sediments. *Geochimica et Cosmochimica Acta* 60(16): 3139-3142.

- Bower, J., Savage, K.S., Weinman, B., Barnett, M.O., Hamilton, W.P., Harper, W.F. (2008). Immobilization of mercury by pyrite (FeS₂). *Environmental Pollution* 156 (2): 504-514.
- Branfireun, B.A., Roulet, N.T., Kelly, C.A., Rudd, J.M. (1999). In situ sulphate stimulation of mercury methylation in a boreal peatland: Toward a link between acid rain and methylmercury contamination in remote environments. *Global Geochemical Cycles* 14(2): 743-750.
- Brendel, P.J. and Luther, G.W. (1995). Development of a gold amalgam voltammetric microelectrode for the determination of dissolved Fe, Mn, O₂, and S(-II) in porewaters of marine and fresh-water sediments. *Environmental Science and Technology* 29(3): 751-761.
- Brown, E.T., Laurence, L.C., et al. (2000). Geochemical cycling of redox sensitive metals in sediments from lake Malawi: a diagnostic paleotracer of episodic changes in mixing depth. *Geochimica et Cosmochimica Acta* 64(20): 3515-3523.
- Brouwer, H. and Murphy, T.P. (1994). Diffusion method for the determination of acid-volatile sulfides (AVS) in sediment. *Environmental Toxicology and Chemistry* 13(8) 1273-1275.
- Burdige, J.D. (2007). Preservation of organic matter in marine sediments: controls, mechanisms, and an imbalance in sediment organic carbon budgets? *Chemical Reviews* 107(2): 467-485.
- Choe, K.Y., Gill, G.A., Lehman, R.D., Han, S., Heim, W.A., Coale, K.H. (2004). Sediment-water exchange of total mercury and mono methylmercury in the San Francisco Bay Delta. *Limnology and Oceanography* 49(5): 1512-1527.
- Choi, S.C., Chase, T., Bartha, R. (1994). Metabolic pathways leading to mercury methylation in *Desulfovibrio desulfuricans* LS. *Applied and Environmental Microbiology* 60(11): 4072-4077.
- Coleman Wasik, J. K., Mitchell, C. P. J., Engstrom, D. R., Swain, E. B., Monson, B. A., Balogh, S., J., Jeremiason, J. D., Branfireun, B., A., Eggert, S. L., Kolka, R. A., and Almendinger, J. E. (2012) Methylmercury declines in a boreal peatland when experimental sulfate deposition decreases. *Environmental Science and Technology* 46(12): 6663-6671.
- Compeau, G.C. and Bartha, R. (1985). Sulfate-reducing bacteria: principal methylators of mercury in anoxic estuarine sediment. *Applied and Environmental Microbiology* 50(2): 498-502.

- Covelli, S., Faganeli, J., Horvat, M., Brambati, A. (1999). Porewater distribution and benthic flux measurements of mercury and methylmercury in the Gulf of Trieste (Northern Adriatic Sea). *Estuarine, Coastal and Shelf Science* 48(4): 415-428.
- Crane, J.L. (2006) Sediment Quality Conditions in the Lower St. Louis River, Minnesota/Wisconsin. MPCA. Report #tdr-fd06-03
- Deonaraine, A., and Hsu-Kim, H. (2009). Precipitation of mercuric sulfide nanoparticles in NOM-containing water: implications for the natural environment. *Environmental Science and Technology*. 43(7): 2368-2373
- DiPasquale, M.M., Agee, J., McGowan, C., Oremland, R.S., Thomas, M., Krabbenhoft, D., Gilmour, C.C. (2000). Methyl-mercury degradation pathways: A comparison among three mercury-impacted ecosystems. *Environmental Science and Technology*. 34(23): 4908-4916
- Drott, A., Lambertsson, L., Bjorn, E., Skyllberg, U. (2007). Importance of dissolved neutral mercury sulfides for methylmercury production in contaminated sediments. *Environmental Science and Technology* 41(7): 270-2276.
- Drott, A., Lambertsson, L., Bjorn, E., Skyllberg, U. (2008). Do potential methylation rates reflect accumulated methylmercury in contaminated sediments? *Environmental Science and Technology* 42(1): 153-158.
- Eaton, D.A., Clesceri, L.S., et al. (2005). Standard Methods for the Examination of Water & Wastewater – 4500-S²⁻ G. Ion-Selective Electrode Method. American Public Health Association.
- Emmerson, S.R. and Hedges, J.I. (2008). *Chemical Oceanography and the Marine Carbon Cycle*. Cambridge University Press.
- Fitzgerald, W.F., Lamborg, C.H., and Hammerschmidt, C.R. (2007) Marine biogeochemical cycling of mercury. *Chemical Reviews* (107)641-662.
- Fitzgerald, W.F., Engstrom, D.R., et al. (1998). The case for atmospheric mercury contamination in remote areas. *Environmental Science and Technology* 32(1): 1-7.
- Flemming, E.J., Mack, E.E., Green, P.G., Nelson, D.C. (2006). Mercury methylation from unexpected Sources: molybdate-inhibited freshwater sediments and an iron-reducing bacterium. *Applied and Environmental Microbiology* 72(1): 457-464.
- Fossing, H., Berg, P., et al. (2004). A model set-up for an oxygen and nutrient flux model for Aarhus Bay (Denmark). National Environmental Research Institute.

- Froelich, P.N., Klinkhammer, G.P., Bender, M.L., Luedtke, N.A., Heath, G.R., Cullen, D., Daulphin, P., Hammond, D., Hartman, B., Maynard, V. (1979). Early oxidation of organic matter in pelagic sediments of the eastern equatorial Atlantic: suboxic diagenesis. *Geochimica et Cosmochimica Acta* 43(7): 1075-1090.
- Gill, G.A., Bloom, N.S., Capellino, S., Driscoll, C.T., Dobbs, C., McShea, L., Mason, R., Rudd, J.M. (1999). Sediment-water fluxes of mercury in Lavaca Bay, Texas. *Environmental Science and Technology*. 33(5): 663-669.
- Gilmour, C.C., Henry, E.A., Mitchell, R. (1992). Sulfate stimulation of mercury methylation in fresh-water sediments. *Environmental Science and Technology* 26(11): 2281-2287.
- Gilmour, C.C., Riedel, G.S., Ederington, M.C., Bell, J.T., Benoit, J.M., Gill, G.A., Stordal, M.C. (1998). Methylmercury concentrations and production rates across a trophic gradient in the northern Everglades. *Biogeochemistry* 40(2-3): 217-345.
- Golding, G.R., Kelly, C.A., Sparling, R., Loewen, P.C., Rudd, J.M., Barkay, T. (2002). Evidence for facilitated uptake of Hg(II) by *Vibrio anguillarum* and *Escherichia coli* under anaerobic and aerobic conditions. *Limnology and Oceanography* 47(4): 967-975.
- Graham, A.M., Aiken, G.R., Gilmour, C.C. (2012). Dissolved organic matter enhances microbial methylation under sulfidic conditions. *Environmental Science and Technology* 36(5): 2715-2723.
- Hammerschmidt, C.R. and Fitzgerald W.F. (2001). Formation of artifact methylmercury during extraction from a sediment reference material. *Analytical Chemistry*. 73(24): 5930-5936.
- Hammerschmidt, C.R. and Fitzgerald, W.F. (2004^a). Geochemical controls on the production and distribution of methylmercury in near-shore marine sediments. *Environmental Science and Technology* 38(5): 1487-1495.
- Hammerschmidt, C.R., Fitzgerald, W.F., Lamborg, C.H., Balcom, P.H. Visscher, P.T. (2004^b). Biogeochemistry of methylmercury in sediments of Long Island Sound. *Marine Chemistry* 90(1-4): 31-52.
- Hammerschmidt, C.R. and Fitzgerald, W.F. (2008). Sediment-water exchange of methylmercury determined from shipboard benthic flux chambers. *Marine Chemistry* 109(1-2): 86-97.

- Hammerschmidt, C.R. and Burton, B. A. (2010). Measurements of acid volatile sulfide and simultaneously extracted metals are irreproducible among laboratories. *Environmental Toxicology and Chemistry*. 29 (8): 1781-1787.
- Harmon, S.M., King, J.K., Gladden, J.B., Chandler, G.T., Newman, L.A. (2004). Methylmercury formation in a wetland mesocosm amended with sulfate. *Environmental Science and Technology* 38(2): 650-656.
- Harmon, S.M., King, J.K., Gladden, J.B., Newman, L.A. (2007). Using sulfate-amended sediment slurry batch reactors to evaluate mercury methylation. *Archives of Environmental Contamination and Toxicology* 52(3): 326-331.
- Hawkins, R.J. and Purdy, K.J. (2007). Genotypic distributions of an indigenous model microorganism along an estuarine gradient. *FEMS Microbiology Ecology* 62(2): 187-197.
- Hicks, R.E. and Oster, R.J. (2012). Developing a risk assessment tool to predict the risk of accelerated corrosion to port infrastructure. *Great Lakes Maritime Research Institute* 1-20.
- Hines, N.A., Brezonik, P.L., Engstrom, D.R. (2004). Sediment and porewater profiles and fluxes of mercury and methylmercury in a small seepage lake in northern Minnesota. *Environmental Science and Technology* 38: 6610-6617.
- Hintelmann, H. and Evans, R.D. (1997). Application of stable isotopes in environmental tracer studies – Measurement of monomethylmercury (CH₃Hg⁺) by isotope dilution ICP-MS and detection of Species transformation. *Fresenius Journal of Analytical Chemistry* 358(2): 378-385.
- Hintelmann, H. and Ogrinc, N. (2003). Determination of stable mercury isotopes by ICP/MS and their applications in environmental studies. *Biogeochemistry of Environmentally Important Trace Elements – ACS Symposium Series 835*: 321-338.
- Horvat, M., Bloom, N.S., Liang, L. (1993). Comparison of distillation with other current isolation methods for determination of methylmercury compounds in low level environmental samples. *Analytica Chimica Acta* 281: 135-152.
- Jeremiason, J.D., Engstrom, D.R., Swain, E.B., Nater, E.A., Johnson, B.M., Almendinger, J.M., Monson, B.A., Kolka, R.K. (2006). Sulfate addition increases methylmercury production in an experimental wetland. *Environmental Science and Technology* 40(12): 3800-3806.

- Jonsson, S., Skjellberg, U., Bjorn, E. (2010). Substantial emission of gaseous monomethylmercury from contaminated water-sediment microcosms. *Environmental Science and Technology* 44(1): 278-283.
- Jorgensen, B.B. (1982). Mineralization of organic matter in the sea bed-the role of sulphate reduction. *Nature* 296(5858): 643-645.
- Katsev, S., Sundby, B., Mucci, A. (2006). Modeling vertical excursions of the redox boundary in sediments: application to deep basins of the Arctic Ocean. *Limnology and Oceanography* 51(4): 1581-1593.
- Kerin, E.J., Gilmour, C.C., Roden, E., Suzuki, M.T., Coates, J.D., Mason, R.P. (2006). Mercury methylation by dissimilatory iron reducing bacteria. *Applied and Environmental Microbiology* 72(12): 7919-7921.
- Kim, M., Han, S., Gieskes, J., Deheyn, D.D. (2011). Importance of organic matter lability for monomethylmercury production in sulfate-rich marine sediments. *Science of the Total Environment* 409(4): 778-784.
- King, J.K., Saunders, F.M., Lee, R.F., Jahnke, R.A. (1999). Coupling mercury methylation rates to sulfate reduction rates in marine sediments. *Environmental Toxicology and Chemistry* 18(7): 2491-2496.
- King, J.K., Kostka, J.E., Frischer, M.E. Saunders, F.M. (2000). Sulfate reducing bacteria methylate mercury at variable rates in pure culture and in marine sediments. *Applied and Environmental Microbiology* 66(6): 2430-2437.
- King, J.K., Kostka, J.E. (2001). A quantitative relationship that demonstrates mercury methylations rates in marine sediments are based on community composition and activity of sulfate reducing bacteria. *Environmental Science and Technology* 34(12): 2491-2496.
- Krom, M.D. and Berner, R.A. (1980). The diffusion-coefficients of sulfate, ammonium, and phosphate ions in anoxic marine sediments. *Limnology and Oceanography* 25(2): 327-337.
- Lambertsson, L. and Nilsson, M. (2006). Organic material: The primary control on mercury methylation and ambient methylmercury concentrations in estuarine sediments. *Environmental Science and Technology* 40(6): 1822-1829.
- Lindgren, J., Schuldt, N., Borkholder, B., Howes, T., Levar, A., Olson, C., Tillman J. and Vogt, D. (2006). A study of the St. Louis River. Minnesota Department of Natural Resources Division of Fisheries Report, Duluth, MN.

- Liu, J.R., Valsaraj, K.T., Delaune., R.D. (2008). Inhibition of Mercury Methylation by Iron Sulfides in Anoxic Sediment. *Environmental Engineering Science* 26(4): 833-840.
- Liu, K.K., Kao, S.J., et al. (2007). Carbon and nitrogen isotopic compositions of particulate organic matter and biogeochemical processes in the eutrophic Danshuei Estuary in northern Taiwan. *Science of the Total Environment* 382(1): 103-120.
- Mason, R.P., Kim, E.H., Cornwell, J., Heyes, D. (2006). An examination of the factors influencing the flux of mercury, methylmercury and other constituents from estuarine sediment. *Marine Chemistry* 102(1-2): 96-110.
- Meyers, P.A. and Ishiwatari, R. (1993). Lacustrine organic geochemistry – an overview of indicators of organic matter sources and diagenesis in lake sediments. *Organic Geochemistry* 20(7): 867-900.
- Miller, C. (2006). The Role of Organic Matter in the Dissolved Phase Speciation and Solid Phase Partitioning of Mercury. Univ. of Maryland. Ph.D. Dissertation.
- Mitchell, C.J., Branfireun, B.A., K.K., Kolka. (2008^a). Assessing sulfate and carbon controls on net methylmercury production in peatlands: An in situ mesocosm approach. *Applied Geochemistry* 23(3): 503-518.
- Mitchell, C.J. and Gilmour, C.C. (2008^b). Methylmercury production in a Chesapeake Bay Salt Marsh. *Journal of Geophysical Research* 113: 1-14.
- Oster, R. J. 2012. Modeling the Corrosive Loss of Port Infrastructure in the Duluth-Superior Harbor and the North Shore of Lake Superior. M.S. thesis. University of Minnesota.
- Phillips, E.J. and Lovely, D.R. (1987). Determination of iron(III) and iron(II) in oxalate extracts of sediment. *Soil Science Society of America Journal* 51(4): 938-941.
- Ratcliffe, H.E., Swanson, G.M., Fischer, L.J. (1996). Human exposure to mercury: a critical assessment of the evidence of adverse health effects. *Journal of Toxicology and Environmental Health* 49(3): 221-270.
- Schaefer, J.K. and Morel., F.M. (2009). High methylation rates of mercury bound to cysteine by *Geobacter sulfurreducens*. *Nature Geoscience* 2(2): 123-126.

- Schaefer, J.K., Rocks, S.S., Zheng, W., Liang, L.Y., Gu, B.H., Morel, F.M.M. (2011). Active transport, substrate specificity, and methylation of Hg(II) in anaerobic bacteria. *Proceedings of the National Academy of Sciences of the United States of America* 108(21): 8714-8719.
- Schippers, A. and Neretin, L.N. (2006). Quantification of microbial communities in near surface and deeply buried sediments on Peru continental margin using real-time-PCR. *Environmental Microbiology* 8: 1251-1260.
- Schulz, H.D. (2000). Quantification of early diagenesis: dissolved constituents in marine porewater. *Marine Geochemistry*. 73-124.
- Sellers, P., Kelly, C.A., Rudd, J.W.M., MacHutchon, A.R. (1996). Photodegradation of methylmercury in lakes. *Nature*. 380(6576): 694-697.
- SLRA. (2002). Lower St. Louis River Habitat Plan. St. Louis River Alliance, Duluth, MN.
- Skyllberg, U. (2008). Competition among thiols and polysulfides for Hg and MeHg in wetland soils and sediments under suboxic conditions: Illuminations of controversies and implications for MeHg net production. *Journal of Geophysical Research-Biogeosciences* 113: 1-14
- Skyllberg, U. and Drott, A. (2010). Competition between Disordered Iron Sulfide and Natural Organic Matter Associated Thiols for Mercury(II)-An EXAFS study. *Environmental Science and Technology* 44(4): 1254-1259
- Stumm, W. and Morgan, J.J. (1996) *Aquatic Chemistry, Chemical Equilibria and Rates in Natural Waters*. Wiley & Sons.
- Torodova, S.G., Driscoll, C.T., et al. (2009). Evidence for regulation of monomethyl mercury by nitrate in a seasonally stratified, eutrophic lake. *Environmental Science and Technology* 43(17): 6572-6578.
- Turner, A, Millward, G.E., Le Roux, S.M. (2001). Sediment-water partitioning of inorganic mercury in estuaries. *Environmental Science and Technology* 35(23): 4648-4645.
- Vannote, R.L., Minshall, G.W., Cummins, K.W., Sedell, J.R., Cushing C.E. (1980). The river continuum concept. *Canadian Journal of Fisheries and Aquatic Sciences* 37(1): 130.

- Wasik, J.K.C., Mitchell, C.P.J., Engstrom, D.R., Swain, E.B., Monson, B.A., Balogh, S.J., Jeremiason, J.D., Branfireun, B.A., Eggert, S.L., Kolka, R.K., Almendinger, J.E. (2012). Methylmercury declines in a boreal peatland when experimental sulfate deposition decreases. *Environmental Science and Technology*. 46(12): 6663-6671.
- Wetzel, R.G. (2002). *Limnology, Third Edition: Lake and River Ecosystems*. Elsevier Science. 35(23): 4648-4654.
- Wiener, J.G., Knights, B.C., et al. (2006). Mercury in soils, lakes, and fish in Voyageurs National Park (Minnesota): importance of atmospheric deposition and ecosystem factors. *Environmental Science and Technology*. 40(20): 6261-6268.
- Wisconsin Department of Natural Resources. (2011). Fish consumption advice for the St. Louis River area of concern. WI DNR Memo.
- Yu, R.Q., Flanders, J.R., Mack, E.E., Turner, R., Mirza, M.B. Barkay, T. (2012). Contribution of coexisting sulfate and iron reducing bacteria to methylmercury production in freshwater river sediments. *Environmental Science and Technology* 46(4): 2684-2691.

Appendix: Supporting Information

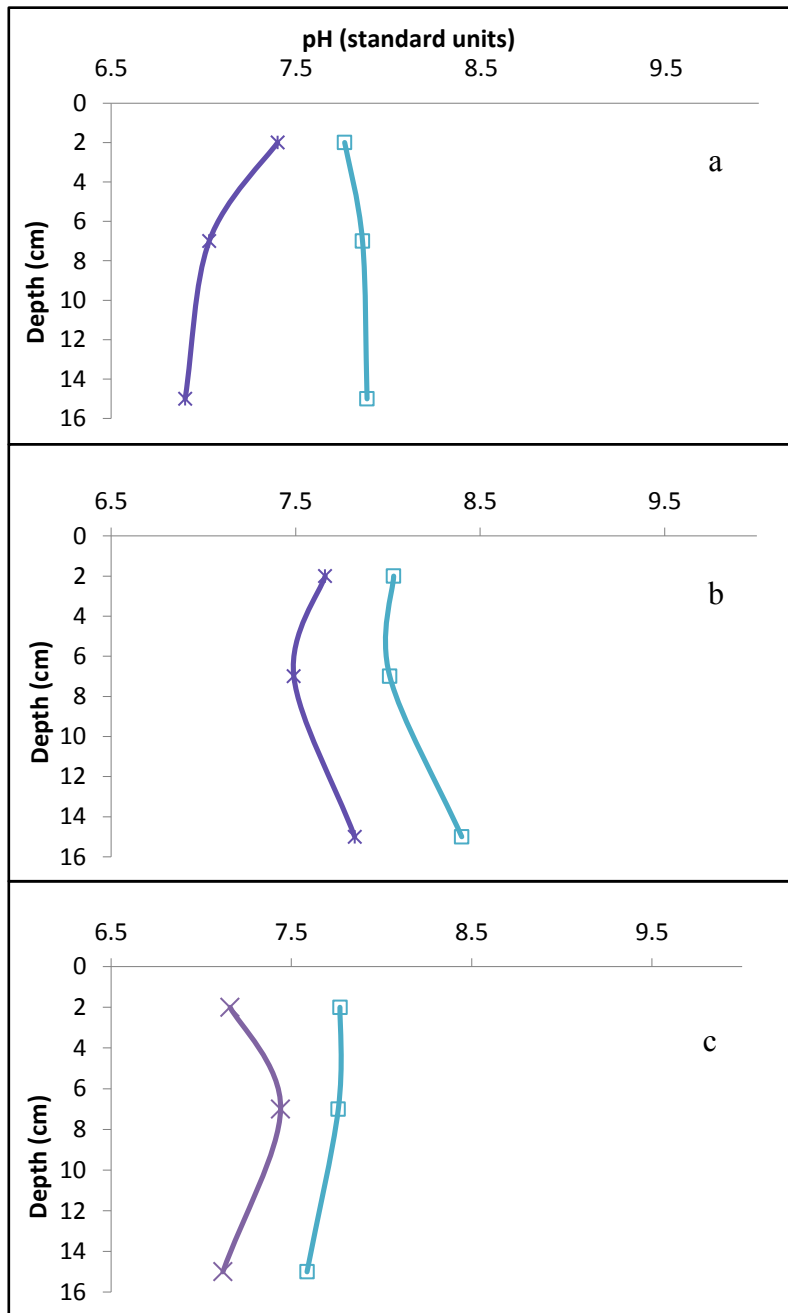


Figure S1 Sediment pH profiles of the initial (empty squares) and final (crosses) conditions for the SB (a), UEF(b), and LEF(c) habitat zones. Final pH measurements were made within a half hour of collection, while initial measurements were made within 3-6 hours of collection.

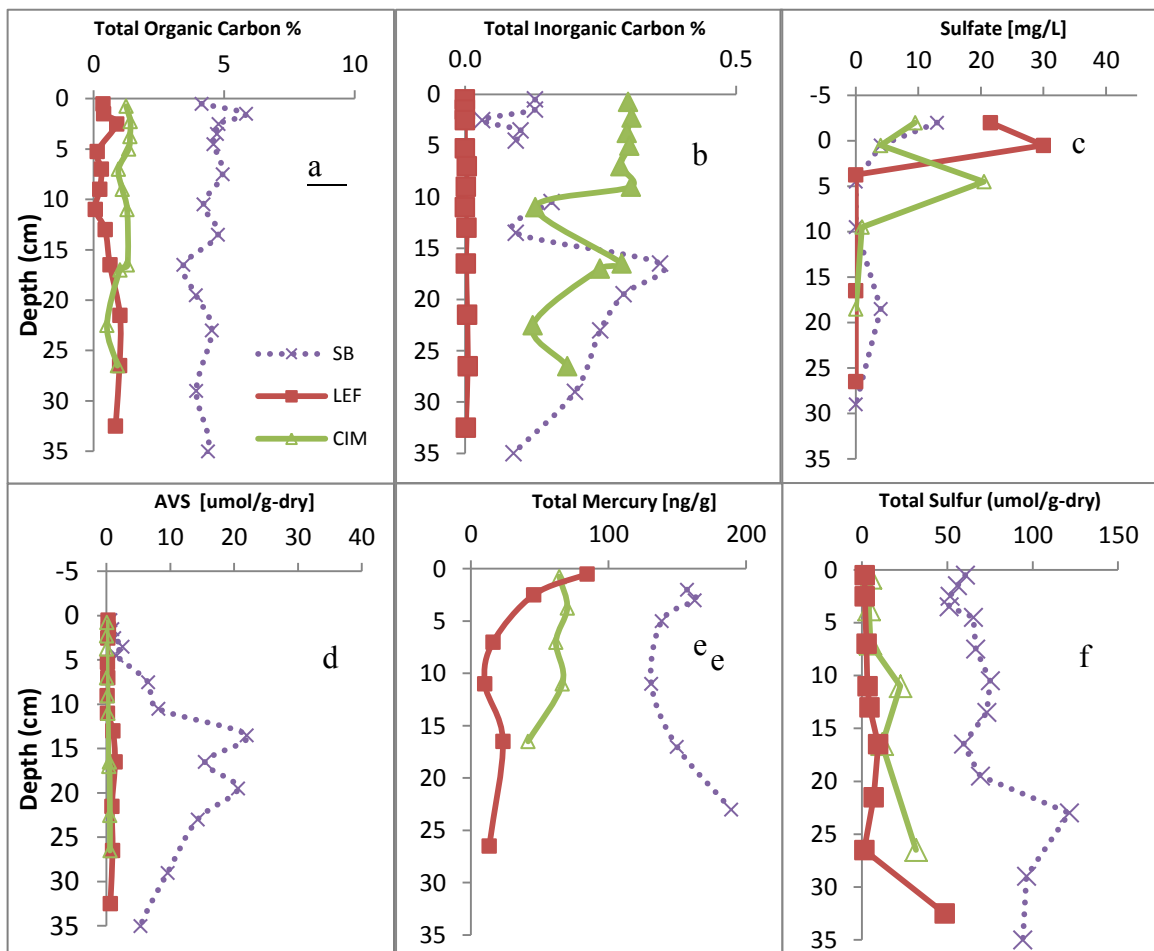


Figure S2 Preliminary data on sediment parameters obtained one year prior to the sulfate addition experiment. Sediment (a) Total organic carbon, (b) total inorganic carbon, (c) porewater sulfate, (d) solid phase AVS, (e) solid phase THg, (f) total sulfur sediment profiles from the Lower Estuary Flats (solid red squares), Clay Influenced Mouth (solid green triangles), and Sheltered Bays (dashed purple crosses).

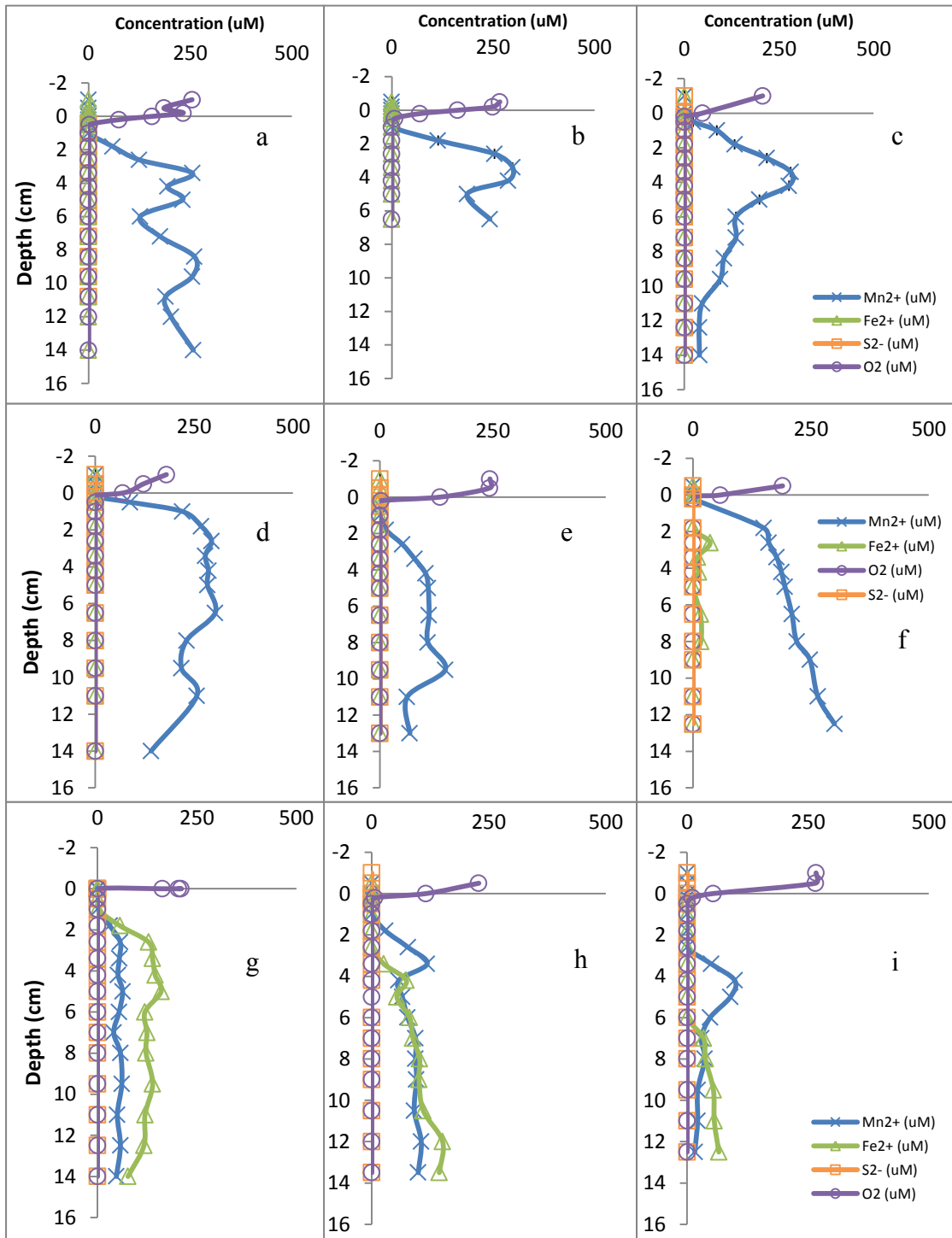


Figure S3 October (+2 months) porewater redox profiles for the LEF ((a)low, (b)control, (c)high), UEF ((d)low, (e)control, and (f)high), and SB ((g)low, (h)control, and (i)high) microcosms. A solid black line (0 cm) denotes the sediment water interface on each sediment profile.

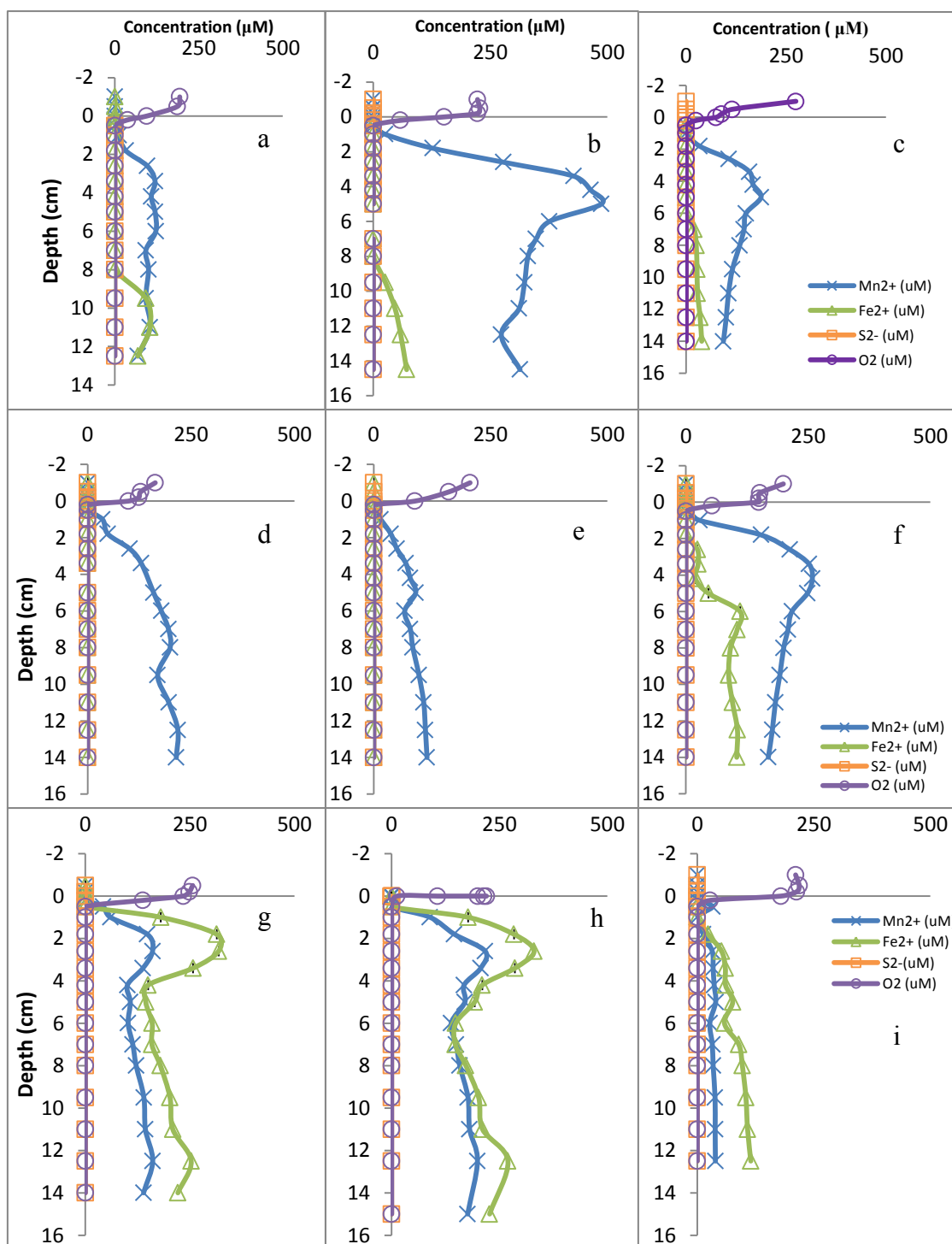


Figure S4 January (+4 months) porewater redox profiles for the LEF ((a)low, (b)control, (c)high), UEF ((d)low, (e)control, and (f)high), and SB ((g)low, (h)control, and (i)high) microcosms. A solid black line (0 cm) denotes the sediment water interface on each sediment profile.

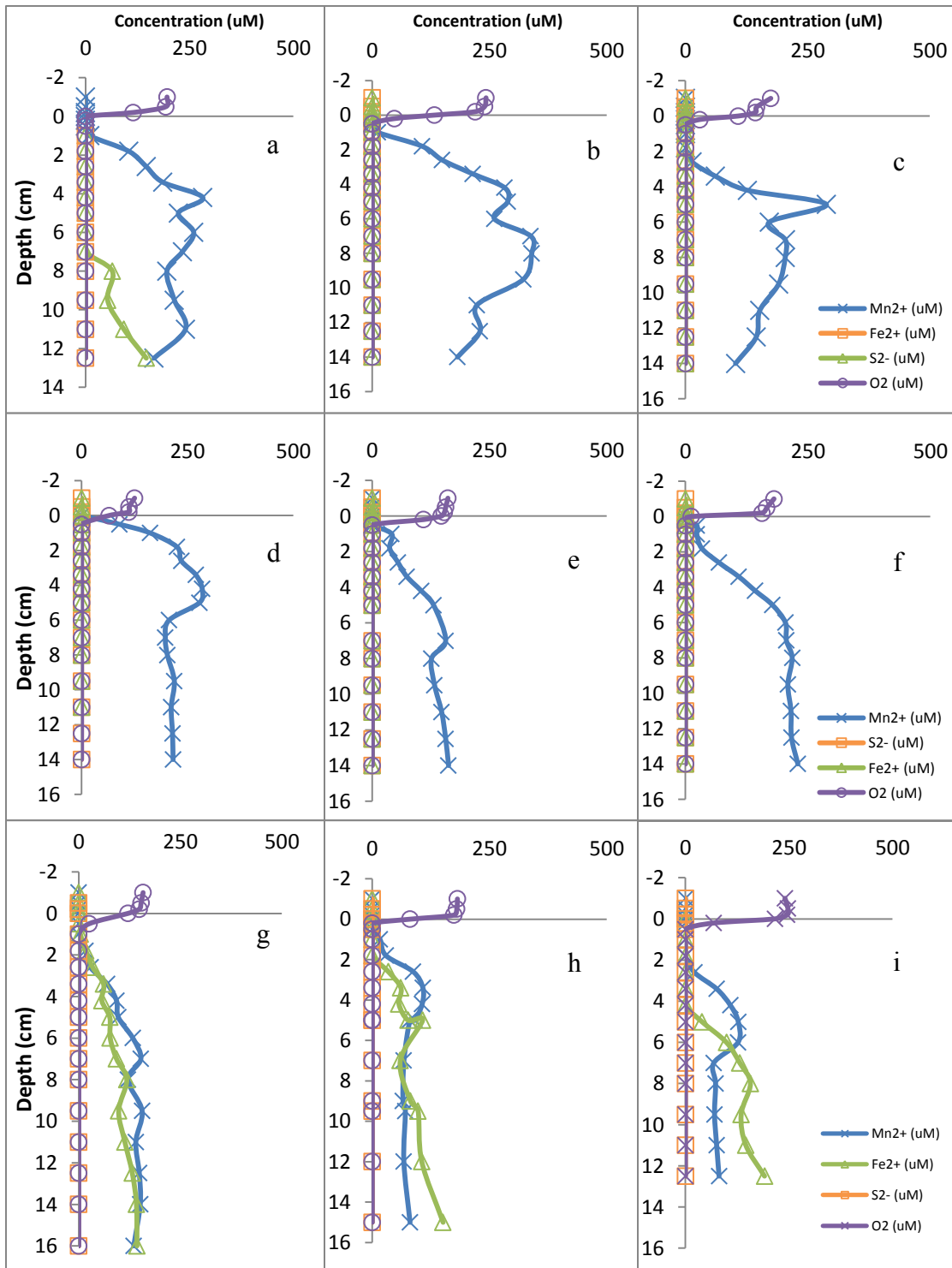


Figure S5 February (+6 months) porewater redox profiles for the LEF ((a)low, (b)control, (c)high), UEF ((d)low, (e)control, and (f)high), and SB ((g)low, (h)control, and (j)high) microcosms. A solid black line (0 cm) denotes the sediment water interface on each sediment profile.

Depth of Sample	Sample	AVS $\mu\text{M g}^{-1}$ dw	THg ng g^{-1} dw	MeHg ng g^{-1} dw	%MeHg ng g^{-1} dw	Chloride mg L^{-1}	Sulfate mg L^{-1}
0-4 cm	SB-4-1-1	57.01	1.80	165.5	1.09	9.85	0.00
4-10 cm	SB-4-2-1	34.29	1.04	170.2	0.61	9.14	0.00
10-20 cm	SB-4-3-1	9.77	1.58	237.1	0.67	8.37	0.00
0-4 cm	LEF-4-1-1	2.44	0.93	105.3	0.88	9.85	12.00
4-10 cm	LEF-4-2-1	5.31	0.39	81.9	0.48	9.14	0.00
10-20 cm	LEF-4-3-1	8.79	0.76	65.2	1.17	8.37	0.00
0-4 cm	UEF-3-1-1	1.18	0.60	66.7	0.90	9.89	2.14
4-10 cm	UEF-3-2-1	14.51	0.55	67.7	0.81	9.02	0.00
10-20 cm	UEF-3-3-1	14.92	0.38	45.1	0.85	8.65	0.00

Table S1. AVS, THg, MeHg, %MeHg, Ferrous Iron, dissolved chloride, and dissolved sulfate measured in sacrificial sediment cores used to fill voids created during initial microcosm coring. Each sacrificial microcosm was sub cored to ensure that the geochemical parameters were not markedly different, after which additional sub-cores were used to fill voids created in other microcosms during initial sub-coring.

Table S 2 Temperature, conductivity, dissolved oxygen (DO), and pH measurements from the overlying water of each sediment core immediately after cores were returned to the lab after field sampling. The LEF and SB habitat zones did not have dissolved oxygen (DO), Conductivity, or temperature recorded during sampling.

Site	Temp (°C)	Conductivity (µS/cm)	DO (mg/L)	pH
UEF 1	24.75	180.2	7.17	7.23
UEF 2	24.7	180.2	7.34	7.22
UEF 3	24.67	180.5	7.42	7.2
UEF 4	25.22	180.8	7.86	7.28
LEF 1	n/r	n/r	n/r	7.86
LEF 2	n/r	n/r	n/r	7.83
LEF 3	n/r	n/r	n/r	7.83
LEF 4	n/r	n/r	n/r	7.6
SB 1	n/r	n/r	n/r	7.71
SB 2	n/r	n/r	n/r	7.92
SB 3	n/r	n/r	n/r	7.61
SB 4	n/r	n/r	n/r	8.12

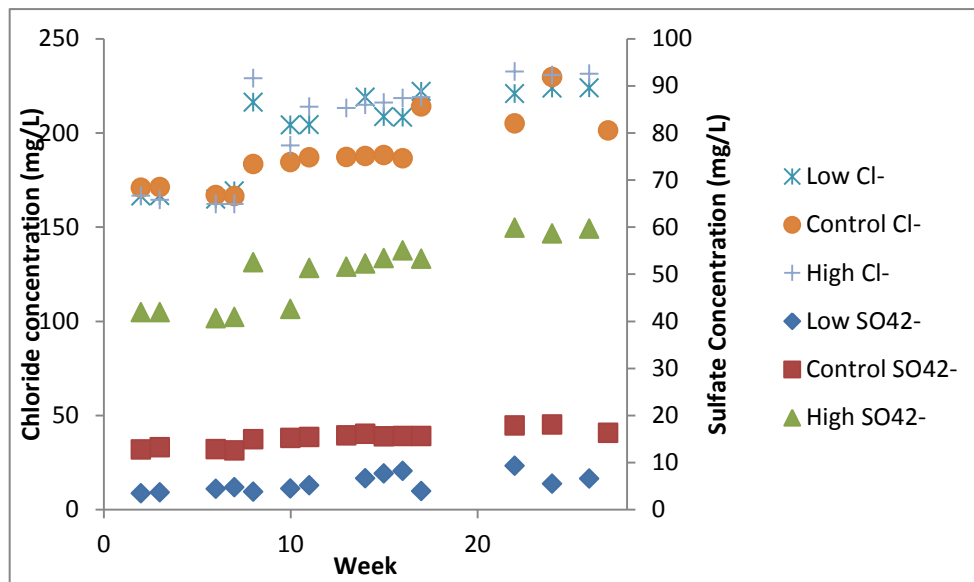


Figure S6 Overlying water in each microcosm was monitored for sulfate and chloride on a bi-weekly basis and is depicted in this figure.

Table S3. Solid phase and porewater MeHg concentrations from the top 10 cm of each microcosm, which were used to calculate a partition coefficient for each habitat zone.

Sample Name	Porewater MeHg [ng/L]	Solid Phase MeHg [ng/g]	Log (k_D)
UEF low	0.28	0.50	3.24
UEF-Control	2.50	0.53	2.32
UEF-High	0.38	0.53	3.14
SB-Low	0.30	1.47	3.69
SB-Control	0.36	1.22	3.52
SB-High	0.30	1.57	3.72
LEF -Low	0.22	1.05	3.68
LEF-Control	0.07	0.37	3.69
LEF- High	1.09	0.87	2.90

Table S4 Solid phase and porewater THg concentrations from the top 10 cm of each microcosm, which were used to calculate a partition coefficient for each habitat zone.

Sample Name	Porewater THg [ng/L]	Solid Phase THg [ng/g]	Log k_D
UEF low part	10.97	70.39	3.80
UEF-Med part	18.17	115.3	3.80
UEF-High-part	7.66	81.79	4.02
SB-Low part	4.51	205.83	4.66
SB-Med-part	6.27	204.64	4.51
SB-High-part	2.67	218.83	4.91
LEF -Low part	50.77	237.9	3.67
LEF-Med-part	9.76	81.37	3.92
LEF-High part	18.34	211.27	4.06